Journal of Advanced Research 53 (2023) 199–218

Contents lists available at ScienceDirect

Journal of Advanced Research

journal homepage: www.elsevier.com/locate/jare

Original Article

Extracellular vesicle-derived CircWhsc1 promotes cardiomyocyte proliferation and heart repair by activating TRIM59/STAT3/Cyclin B2 pathway

Guoquan Wei [a,b], Chuling Li [a,b], Xiaoqian Jia [a,b], Jingfang Xie [a,b], Zhenquan Tang [a,b], Ming Jin [a,b], Qiqi Chen [a,b], Yili Sun [a,b], Sisi He [a,b], Xinzhong Li [a,b], Yanmei Chen [a,b], Hao Zheng [a,b], Wangjun Liao [c], Yulin Liao [a,b], Jianping Bin [a,b,*], Senlin Huang [a,b,*]

[a] Department of Cardiology, State Key Laboratory of Organ Failure Research, Nanfang Hospital, Southern Medical University, 510515 Guangzhou, China
[b] Guangdong Provincial Key Laboratory of Cardiac Function and Microcirculation, 510515 Guangzhou, China
[c] Department of Oncology, Nanfang Hospital, Southern Medical University, 510515 Guangzhou, China

HIGHLIGHTS

- Hypoxia-induced circWhsc1 in neonatal cardiac endothelial cells promotes cardiac regenerative repair by activating TRIM59/STAT3/cyclin B2 pathway.
- CircWhsc1 was secreted by neonatal cardiac endothelial cells in an extracellular vesicle-dependent manner to promote cardiomyocyte proliferation.
- Intercellular circWhsc1 delivery by extracellular vesicles might be a plausible alternative strategy for inducing cardiac regenerative repair.

GRAPHICAL ABSTRACT

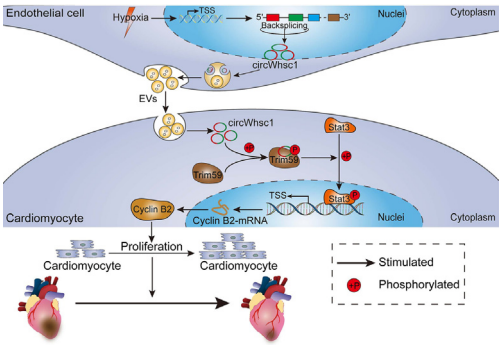

ARTICLE INFO

Article history:
Received 13 October 2022
Revised 22 December 2022
Accepted 26 December 2022
Available online 29 December 2022

Keywords:
CircRNA
Cardiac regeneration
Extracellular vesicle
Endothelial cell

ABSTRACT

Introduction: Extracellular vesicles (EVs)-mediated cell-to-cell communication is crucial for hypoxia-induced cell proliferation and tissue repair, but its function in endogenous cardiac regeneration is still unknown.
Objectives: Herein, we aimed to determine whether hypoxia-inducible circWhsc1 in endothelial EVs promoted cardiomyocyte (CM) proliferation and cardiac regeneration.
Methods: RNA-sequence data was used to identify EV circRNAs that were involved into endogenous cardiac regeneration. Quantitative polymerase chain reactions were conducted to determine circRNA expression in tissue, cells and EVs. Gain- and loss-of-function assays were performed to explore the function of EV-derived circWhsc1 during cardiac regeneration. Western blotting and RNA pulldown assays were used to investigate its underlying mechanism.
Results: We found that circWhsc1 was enriched in neonatal mouse hearts, particularly in cardiac ECs, and was further upregulated both in ECs and EC-derived EVs under hypoxic conditions. When cocultured with hypoxia-preconditioned neonatal ECs or their secreted EVs, both neonatal and adult CMs exhibited an increased proliferation rate and G2/M ratio, which could be attenuated by knockdown of circWhsc1 in ECs. *In vivo*, EC-restricted overexpression of circWhsc1 and EV-mediated delivery of circWhsc1 induced

Peer review under responsibility of Cairo University.
* Corresponding authors at: Department of Cardiology, State Key Laboratory of Organ Failure Research, Nanfang Hospital, Southern Medical University, 1838 Guangzhou Avenue North, Guangzhou 510515, China.
E-mail addresses: jianpingbin@hotmail.com (J. Bin), huangsenlin11@126.com (S. Huang).

https://doi.org/10.1016/j.jare.2022.12.014
2090-1232/

CM proliferation, alleviated cardiac fibrosis and restored cardiac function following myocardial infarction in adult mice. Mechanistic studies revealed that EV-derived circWhsc1 activated TRIM59 by enhancing its phosphorylation, thereby reinforcing the binding of TRIM59 to STAT3, phosphorylating STAT3 and inducing CM proliferation.

Conclusion: The current study demonstrated that hypoxia-inducible circWhsc1 in EC-derived EVs induces CM proliferation and heart regeneration. EC-CM communication mediated by EV-derived circWhsc1 might represent a prospective therapeutic target for inducing cardiac repair post-myocardial infarction.

Introduction

Reactivation of CM proliferation is a promising approach for CM supplementation and heart regeneration after CM loss, which occurs in many heart diseases, such as acute myocardial infarction (AMI), cardiomyopathy, and heart failure [1]. Environmental hypoxia has recently been corroborated as a critical regulator of CM proliferation and heart regeneration [2]. It is believed that the proliferating CMs in lower vertebrates and embryonic or neonatal mice are protected by their relatively low blood oxygenation level. Exposure to oxygen in the environment after birth results in loss of the proliferative capacity of CMs in mammals [3]. Notably, this lost proliferative capacity in adult mammalian CMs can be restored by gradual exposure to hypoxia, demonstrating that hypoxia is necessary and sufficient for cardiac regeneration [4]. However, direct exposure to hypoxia may increase mortality post-MI by causing side effects such as pulmonary hypertension [5] and central nervous dysfunction [6,7], which could substantially offset the holistic benefit of hypoxia-induced heart regeneration. Interestingly, accumulating mechanistic studies have revealed that activation of hypoxia-induced signaling also induces cellular alterations in the hypoxia regime [8–10]. Thus, modulating key molecular mediators in hypoxia might retain the effect of hypoxia on CM proliferation while avoiding adverse events and may have use in future clinical applications, representing an attractive alternative strategy for cardiac regeneration.

ECs are abundant and vigorous residents of the heart that act as important modulators of neighboring CMs and as the "first responders" to environmental cues, including hypoxia [11]. Via active paracrine factors, EC-CM interactions are closely involved in myocardial development, growth, contractility, and function [12–14]. In addition, beginning in the early stages of hypoxia, ECs generate pronounced paracrine signals to facilitate an overall advantageous milieu for CM survival and heart repair through diverse mechanisms, including pro-angiogenic and anti-apoptotic [15]. Extracellular vesicles (EVs) are extracellular lipid membrane vesicles that have emerged as critical mediators of intercellular communication [16–18]. EVs are widely involved in physiological regulation, such as tissue regeneration [19], and in various disease states [20]. Cardiac ECs secrete EVs to exchange biological messages with CMs, playing an important role in maintaining cardiac homeostasis and function. Recent studies have demonstrated that EVs released from ECs are cardioprotective and improve cardiac function after AMI to an extent comparable with that achieved by their parent cells [21]. Therefore, EV-mediated EC-CM communication might play an essential role in hypoxia-induced cardiac regenerative repair.

Circular RNA (circRNA) is an important class of cargo that is enriched in EVs and participates in intercellular communication and subsequent intracellular signaling modulation [22–25]. Owing to their circular structure, circRNAs are more stable and durable than linear RNAs or proteins that usually have short half-lives, which may allow for more efficient intercellular molecule transport. Comparatively, circRNAs are gaining increasing attention due to their tissue-specific and stable characteristics [20,26]. CircRNAs derived from cardiac EVs exert critical functions in multiple physiological and pathophysiological processes, including cell death, cell senescence, and cell differentiation. Interestingly, our previous studies revealed that circRNAs are also involved in regulating CM proliferation and angiogenesis [27,28]. However, the roles of cardiac EVs and their circRNA cargo in endogenous cardiac regeneration are still uncertain. Herein, we hypothesized that EC-derived EVs could transfer essential circRNAs to mediate EC-CM communication to impact CM proliferation and cardiac regeneration in hypoxic hearts.

In this study, we aimed to identify hypoxia-inducible, endothelial EV-abundant circRNAs that mediate EC-CM communication during endogenous cardiac regeneration. Moreover, we sought to explore whether interference with the identified circRNA promoted myocardial repair and improved cardiac function post-MI in adult mice, also investigating the underlying mechanisms. Our findings may provide a promising alternative strategy for hypoxia-induced endogenous heart regeneration.

Results

Hypoxia-associated circRNA Whsc1 is highly expressed in cardiac ECs

To identify hypoxia-inducible EC circRNAs that might be mitogenic to CM, we intersected the circRNAs from existing high-throughput sequencing data of mammalian hearts [26]. We found 87 circRNAs that were both conserved across different species and differentially upregulated in neonatal rodent hearts compared to adult rodent hearts (Fig. 1A). Combining RNA-sequencing results from ECs [29], we identified 10 circRNAs among that 87 that were upregulated in ECs exposed to hypoxic conditions compared to normoxic conditions (Fig. 1A, B). We also isolated ECs from postnatal 1-day-old (*P*1) mouse hearts and assessed the expression levels of these circRNAs using qRT-PCR assays. CircWhsc1 was the most abundant circRNA in ECs among these 10 candidates (Fig. 1C). Cardiac ECs were isolated from neonatal mouse, and then grown under normoxic conditions or hypoxic conditions for 24 hr. As the master regulators of a homeostatic transcriptional response to hypoxia in virtually all cells, HIF1α level was detected and utilized as an indicator test for cellular hypoxia. Our data showed that HIF1α expression level was significantly increased after hypoxia-precondition, indicating cellular hypoxia episode (Fig. S1A). qRT-PCR assays further confirmed that expression of circWhsc1 was significantly upregulated in cardiac ECs exposed to hypoxia or the hypoxia mimic $CoCl_2$, compared to normoxic conditions (Fig. 1-D-E). We also detected circWhsc1 expression in different cell types isolated from mouse hearts. Compared to CM and cardiac fibroblast (CF), circWhsc1 was more abundant in EC, especially in neonatal heart. And EC was the most sensitive cell type to hypoxia among different isolated cardiac cells, in terms of circWhsc1 upregulation (Fig. 1F). These results suggest that circWhsc1 might be an EC-derived circRNA involved in hypoxia-induced cardiac regeneration.

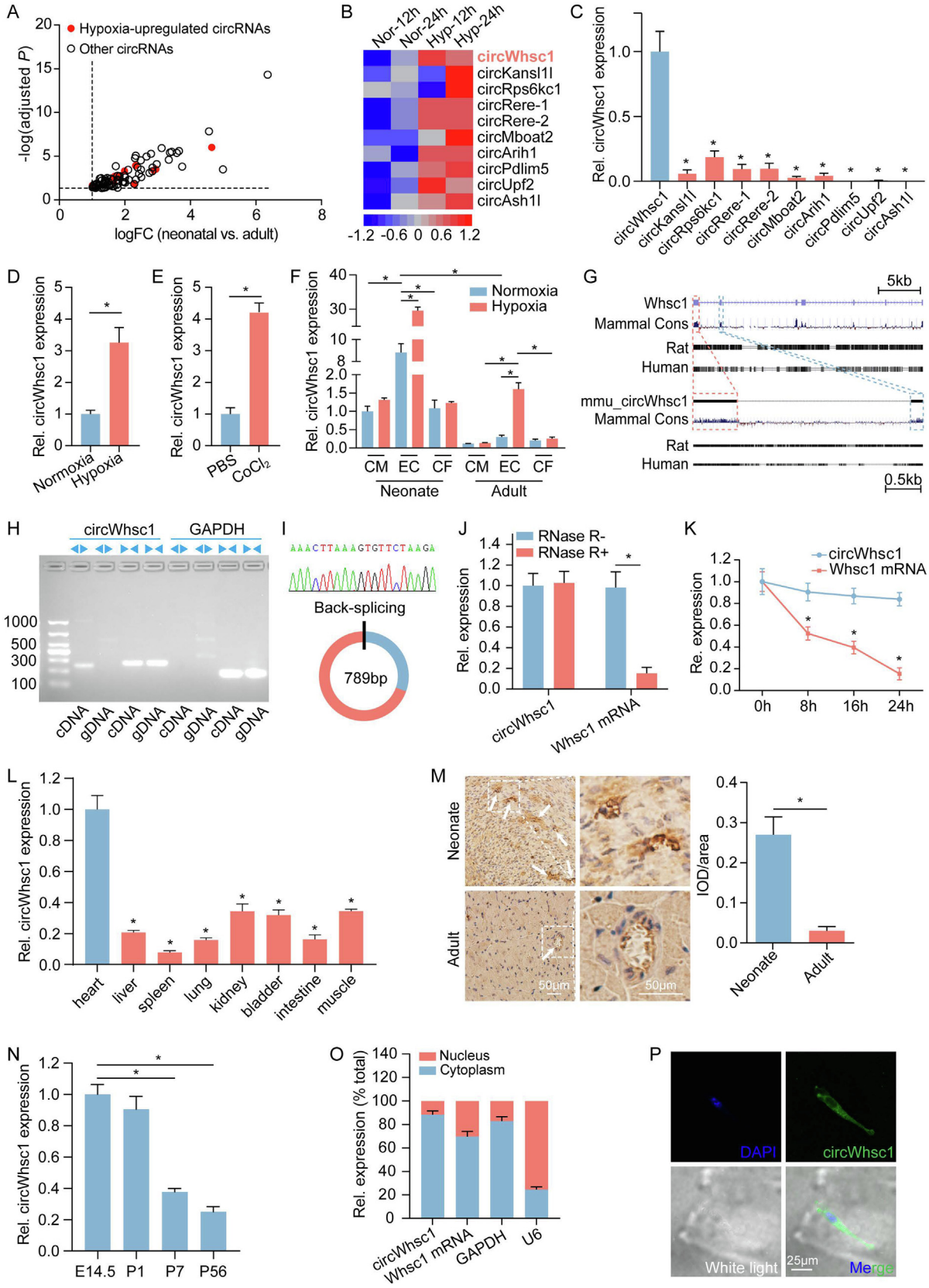
A
Hypoxia-upregulated circRNAs
Other circRNAs
-log(adjusted P)
logFC (neonatal vs. adult)
B
Nor-12h
Nor-24h
Hyp-12h
Hyp-24h
circWhsc1
circKansl1l
circRps6kc1
circRere-1
circRere-2
circMboat2
circArih1
circPdlim5
circUpf2
circAsh1l
C
Rel. circWhsc1 expression
D
Rel. circWhsc1 expression
Normoxia
Hypoxia
E
Rel. circWhsc1 expression
PBS
CoCl2
F
Rel. circWhsc1 expression
Normoxia
Hypoxia
CM EC CF CM EC CF
Neonate
Adult
G
5kb
Whsc1
Mammal Cons
Rat
Human
mmu_circWhsc1
Mammal Cons
Rat
Human
0.5kb
H
circWhsc1
GAPDH
1000
500
300
100
cDNA gDNA cDNA gDNA cDNA gDNA cDNA gDNA
I
AAACTTAAAGTGTTCTAAGA
Back-splicing
789bp
J
RNase R-
RNase R+
Rel. expression
circWhsc1
Whsc1 mRNA
K
circWhsc1
Whsc1 mRNA
Re. expression
0h
8h
16h
24h
L
Rel. circWhsc1 expression
heart
liver
spleen
lung
kidney
bladder
intestine
muscle
M
Neonate
Adult
50μm
50μm
IOD/area
Neonate
Adult
N
Rel. circWhsc1 expression
E14.5
P1
P7
P56
O
Nucleus
Cytoplasm
Rel. expression (% total)
circWhsc1
Whsc1 mRNA
GAPDH
U6
P
DAPI
circWhsc1
White light
25μm
Merge

We subsequently performed detailed investigation of circWhsc1, including expression profiling and functional characterization.

The candidate circRNA circWhsc1 is derived from the first two exons of the Whsc1 gene and has a 789 bp head-to-tail junction ring structure (Fig. 1G). Its nucleotide sequence is highly conserved and homologous among humans, mice, and rats (Fig. S2A-B). The circRNA IDs of circWhsc1 in the circBase database (https://www.circbase.org/) are mmu_circ_0001335 and hsa_circ_0008460. CircWhsc1 amplification using divergent primers specifically designed for head-to-tail junctions succeeded using cDNA but not genomic DNA (Fig. 1H). Subsequent Sanger sequencing further confirmed the head-to-tail junction of circWhsc1 (Fig. 1I). CircRNAs often exhibit good stability due to their ring structure. We next confirmed the stability of circWhsc1 using RNase R digestion and actinomycin D (an inhibitor of transcription) treatment. As shown in Fig. 1J, circWhsc1 displayed good tolerance to RNase R digestion compared to linear whsc1 mRNA. Moreover, the actinomycin D assay revealed that the circularized transcript had a longer half-life than the linear transcript (Fig. 1K). In addition, we isolated different tissues from neonatal mice and found that circWhsc1 was much more enriched in the heart than in several other tissues (Fig. 1L). The results of *in situ* hybrid (ISH) assays further confirmed that circWhsc1 was enriched in cardiac ECs, especially in neonatal heart (Fig. 1M). We then assessed circWhsc1 expression at different stages during cardiac development. Consistent with the RNA sequencing data, circWhsc1 levels were significantly higher in embryonic and *P*1 hearts than in P7 or adult hearts (Fig. 1N). In addition, qRT-PCR and fluorescence *in situ* hybridization (FISH) assays demonstrated that circWhsc1 is primarily enriched in the cytoplasm of ECs (Fig. 1O-P).

Hypoxia-induced circWhsc1 promotes CM cell cycle progression by mediating intercellular communication

To determine the effect of hypoxia-induced EC-derived circWhsc1 on CM proliferation, neonatal mouse CMs and ECs were isolated and cocultured using a 0.4 μm pore diameter transwell system (Fig. S3A). One group of ECs was hypoxia-preconditioned for 24 hr before coculture (HP-ECs), with normoxia-preconditioned ECs (NP-ECs) serving as controls. Compared to CMs cultured individually or cocultured with NP-ECs, CMs cocultured with HP-ECs exhibited higher circWhsc1 expression (Fig. S3B), which indicated that the upper layer HP-EC-derived circWhsc1 might transfer to the CMs in the lower layer. To determine whether EC-derived circWhsc1 is involved in regulating CM proliferation, small interfering RNAs (siRNAs) targeting the back-splicing site of circWhsc1 were designed (Fig. S3C). qRT–PCR assays showed that siRNA transfection significantly reduced circWhsc1 expression in cardiac ECs (Fig. S3D) and abolished the circWhsc1 increment effect of the upper layer HP-ECs traversing to the lower layer CMs in the coculture system (Fig. S3B).

We found that CMs cocultured with HP-ECs exhibited superior proliferative capacity, expressing increased cell cycle activity markers, including EdU, Ki67, pH3, and Aurora B (Fig. 2A-C, Fig. S3E). Flow cytometry assays further revealed that CMs cocultured with HP-ECs accumulated in the G2/M phases, while the percentage of cells in the G0/G1 phases of the cell cycle was reduced (Fig. 2D). However, the proliferative signal induced by HP-ECs was impaired when circWhsc1 expression was knocked down using siRNA (Fig. 2A-D, Fig. S3E). Moreover, we isolated CMs from adult mouse hearts and investigated whether coculture with HP-ECs promotes the proliferation of adult mouse CMs. At this stage, proliferation was nearly undetectable in the control adult CMs. Immunofluorescence assays confirmed that HP-EC coculture also promoted adult CM proliferation with an increased Ki67- and pH3-positive adult CM ratio (Fig. S3F-G). We also observed that these proliferating CMs underwent dedifferentiation characterized by partial disassembly of sarcomeres, consistent with previous study [30]. Consistently, downregulation of circWhsc1 reversed the effect of HP-EC coculture on adult CM proliferation (Fig. S3F-G). We further isolated adult cardiac ECs which also was divided into adult HP-ECs group and adult NP-ECs group. Compared to CMs cultured individually or cocultured with adult NP-ECs, CMs cocultured with adult HP-ECs exhibited higher circWhsc1 expression and superior proliferative capacity (Fig. S4A-B). These results revealed that EC-derived circWhsc1 plays a crucial role in the proliferative effect on CMs.

Overexpression of circWhsc1 in cardiac ECs induces adult CM proliferation and angiogenesis *in vivo*

To explore the proliferative effect of EC-derived circWhsc1 *in vivo*, adeno-associated viral (AAV) serotype 2-based serotypes that specifically target EC using the TIE promoter were designed to overexpress circWhsc1 (AAV2-V_{EC}-circWhsc1). AAV2-V_{EC}-circWhsc1 and AAV2-V_{EC}-NC were delivered to adult mouse hearts *in situ*, and green fluorescent protein (GFP)-based assays were conducted to confirm that these viruses specifically transfected cardiac microvascular ECs (Fig. S5A). qRT-PCR assays indicated that AAV2-V_{EC}-circWhsc1 transfection significantly increased circWhsc1 expression in myocardial tissue compared to that in the AAV2-V_{EC}-NC group (Fig. S5B). Similar to *in vitro* assays, immunofluorescence analysis revealed that overexpression of EC-derived circWhsc1 increased the proportion of CMs expressing proliferative markers, including Ki67 and pH3, in adult mouse hearts (Fig. 3A-B). Additionally, wheat germ agglutinin (WGA) staining indicated that overexpression of EC-derived circWhsc1 had no obvious effect on CM hypertrophy (Fig. S5C).

Fig. 1. CircWhsc1, a hypoxia-inducible circRNA, is highly expressed in cardiac ECs. (A) Screened circRNAs that are highly expressed in neonatal rodent hearts, compared to adult rodent hearts. Red dots represent hypoxia-upregulated circRNAs in ECs. (B) Heatmap of circRNAs which are upregulated in ECs after hypoxia treatment, compared to normoxia condition. The upregulated circRNAs are from the hypoxia-upregulated circRNA cluster shown in panel A. Nor, normoxia; Hyp, hypoxia. (C) Relative expression of hypoxia-upregulated circRNAs in isolated neonatal cardiac ECs. $^*P < 0.05$ vs circWhsc1, n = 4. (D) Relative expression of circWhsc1 in cardiac ECs under normoxic or hypoxic conditions. $^*P < 0.05$, n = 6. (E) Relative expression of circWhsc1 in cardiac ECs under PBS treatment or $CoCl_2$ treatment (100 nM). $CoCl_2$ was used to mimic a hypoxic environment. $^*P < 0.05$, n = 6. (F) Relative expression of circWhsc1 in isolated neonatal and adult cardiomyocytes (CMs), cardiac endothelial cells (ECs) and cardiac fibroblasts (CFs) in normoxic or hypoxic environments. $^*P < 0.05$, n = 6. (G) Species conservation analysis of the circWhsc1 sequence using the UCSC Genome Browser. (H) Amplification of circWhsc1 in cDNA but not genomic DNA using divergent primers; gDNA, genomic DNA. (I) Sanger sequencing revealed the head-to-tail junction of circWhsc1. (J) CircWhsc1 and Whsc1 mRNA expression levels in ECs after RNase R treatment. $^*P < 0.05$, n = 4. (K) CircWhsc1 and Whsc1 mRNA expression levels in ECs after actinomycin D treatment; $^*P < 0.05$ vs Whsc1 mRNA at each time point, n = 4. (L) Relative expression of circWhsc1 in different organs from neonatal mice. $^*P < 0.05$, n = 3. (M) ISH analysis of circWhsc1 abundance in neonatal and adult mouse hearts, Scale bars, 50 μm. (N) Relative expression of circWhsc1 in hearts from embryonic (E) 14.5, postnatal (P)1, P7, and P56 mice. $^*P < 0.05$, n = 4. (O) Proportion of CircWhsc1 and Whsc1 mRNA expression in the nucleus and cytoplasm of ECs. n = 4. (P) RNA-FISH assays of circWhsc1 distribution in ECs, Scale bars, 25 μm. (For interpretation of the references to colour in this figure legend, the reader is referred to the web version of this article.)

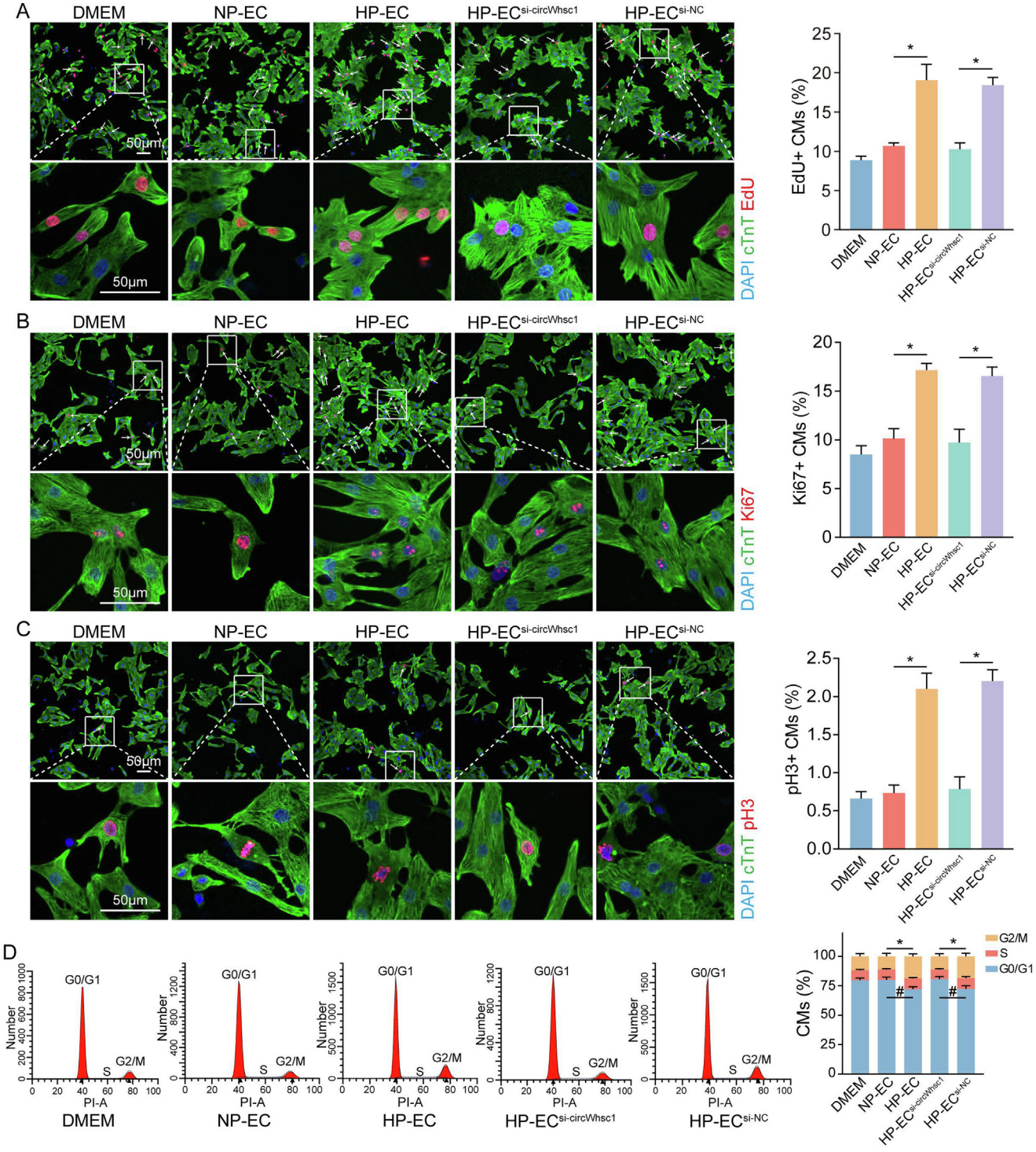

Fig. 2. CircWhsc1 down-regulation suppresses the promoting effect of hypoxia-treated ECs on CM proliferation in coculture. (A-C) Representative immunofluorescence images and quantification of EdU- (A), Ki67- (B), and pH3- (C) positive CMs. One-day-old (*P*1) mouse CMs were cultured *in vitro* individually (DMEM) or cocultured with normoxia-preconditioned ECs (NP-ECs), hypoxia-preconditioned ECs (HP-ECs), hypoxia-preconditioned ECs treated with si-circWhsc1 (HP-EC$^{si\text{-}circWhsc1}$), and hypoxia-preconditioned ECs treated with si-NC (HP-EC$^{si\text{-}NC}$). CMs are stained with cTnT, nuclei are labeled with DAPI, and arrows indicate proliferating CMs. $^{*}P < 0.05$, n = 6. Scale bars, 50 μm. (D) Flow cytometry analysis of CM cell cycle events. $^{*}P < 0.05$ in G2/M phase, $\#P < 0.05$ in G0/G1 phase, n = 6.

The ability of EC-derived circWhsc1 to promote CM proliferation in adult mice raises the question of whether it can increase the repair capacity of the adult heart after injury. To address this question, we performed MI by permanent left anterior descending (LAD) ligation in 8-week-old mice and intramyocardially injected either AAV2-V_{EC}-circWhsc1 or AAV2-V_{EC}-NC into the *peri*-infarcted area immediately after surgery. The results showed that compared to the control group, EC-derived circWhsc1 overexpression markedly elevated the ratio of proliferative CMs in the *peri*-infarcted zone 14 days post-MI (Fig. 3C–D). In addition to the proliferative effect on CMs, we sought to examine whether EC-derived circWhsc1 would be beneficial to angiogenesis. Cluster of differen-

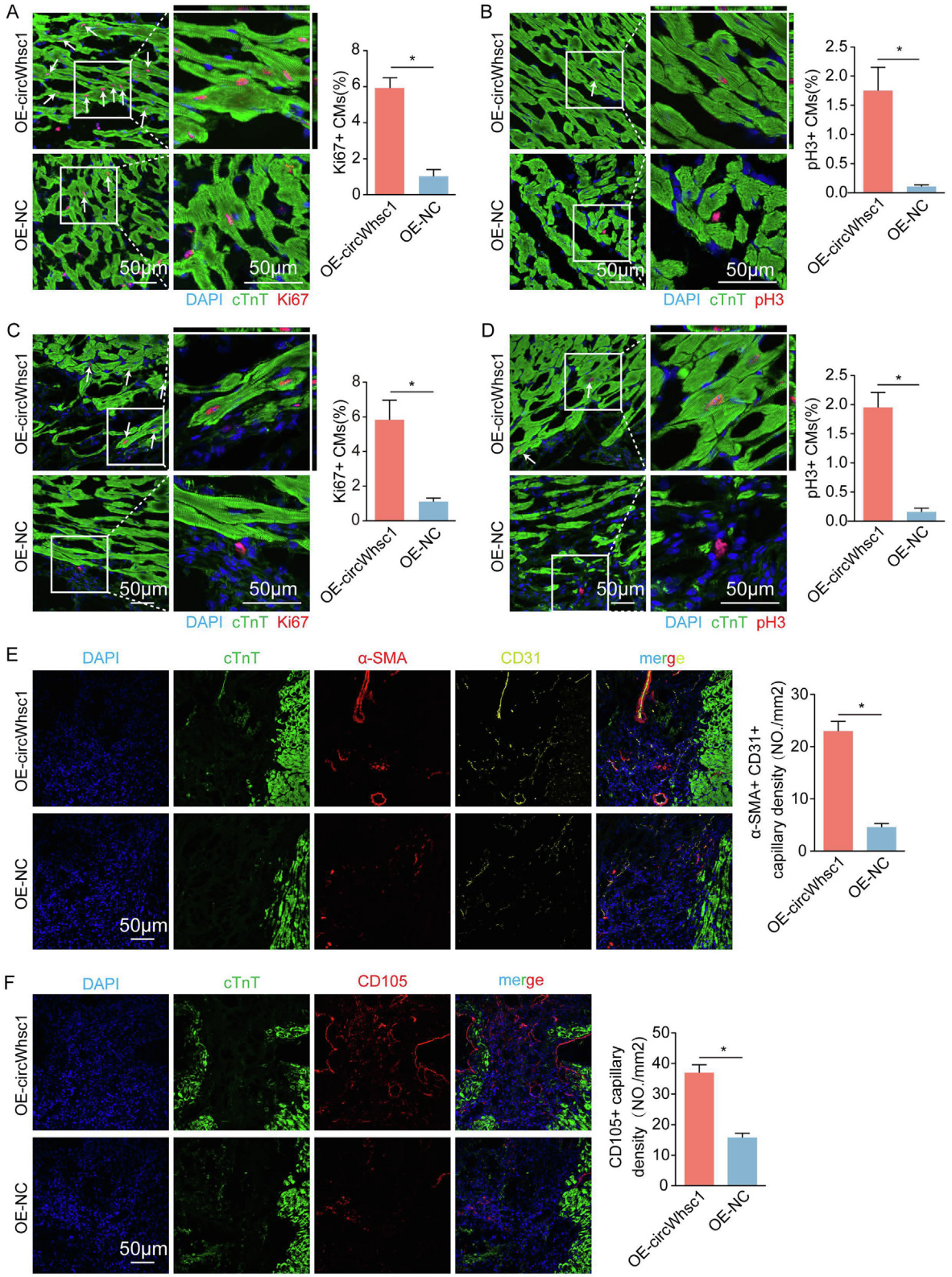

Fig. 3. Cardiac endothelial circWhsc1 overexpression promotes CM proliferation and angiogenesis *in vivo*. (A-B) Immunofluorescence analysis of Ki67- (A) and pH3- (B) positive adult CMs in heart sections 14 days after AAV2-V_{EC}-circWhsc1-GFP or AAV2-V_{EC}-NC injection. CMs are stained with cTnT, nuclei are labeled with DAPI, and proliferating CMs are indicated by arrows, $^{*}P < 0.05$, n = 6. Scale bars, 50 μm. (C-D) Immunofluorescence analysis of Ki67- (C) and pH3- (D) positive adult CMs in the *peri*-infarcted area of the OE-circWhsc1 and OE-NC group 14 days post MI. Proliferating CMs are indicated by arrows, $^{*}P < 0.05$, n = 6. Scale bars, 50 μm. (E) CD31 and α-SMA costaining in the *peri*-infarcted zone 14 days after AAV2-V_{EC}-circWhsc1-GFP or AAV2-V_{EC}-NC injection. $^{*}P < 0.05$, n = 6. Scale bars, 50 μm. (F) CD105 staining in the *peri*-infarcted zone 14 days after AAV2-V_{EC}-circWhsc1-GFP or AAV2-V_{EC}-NC injection. $^{*}P < 0.05$, n = 6. Scale bars, 50 μm.

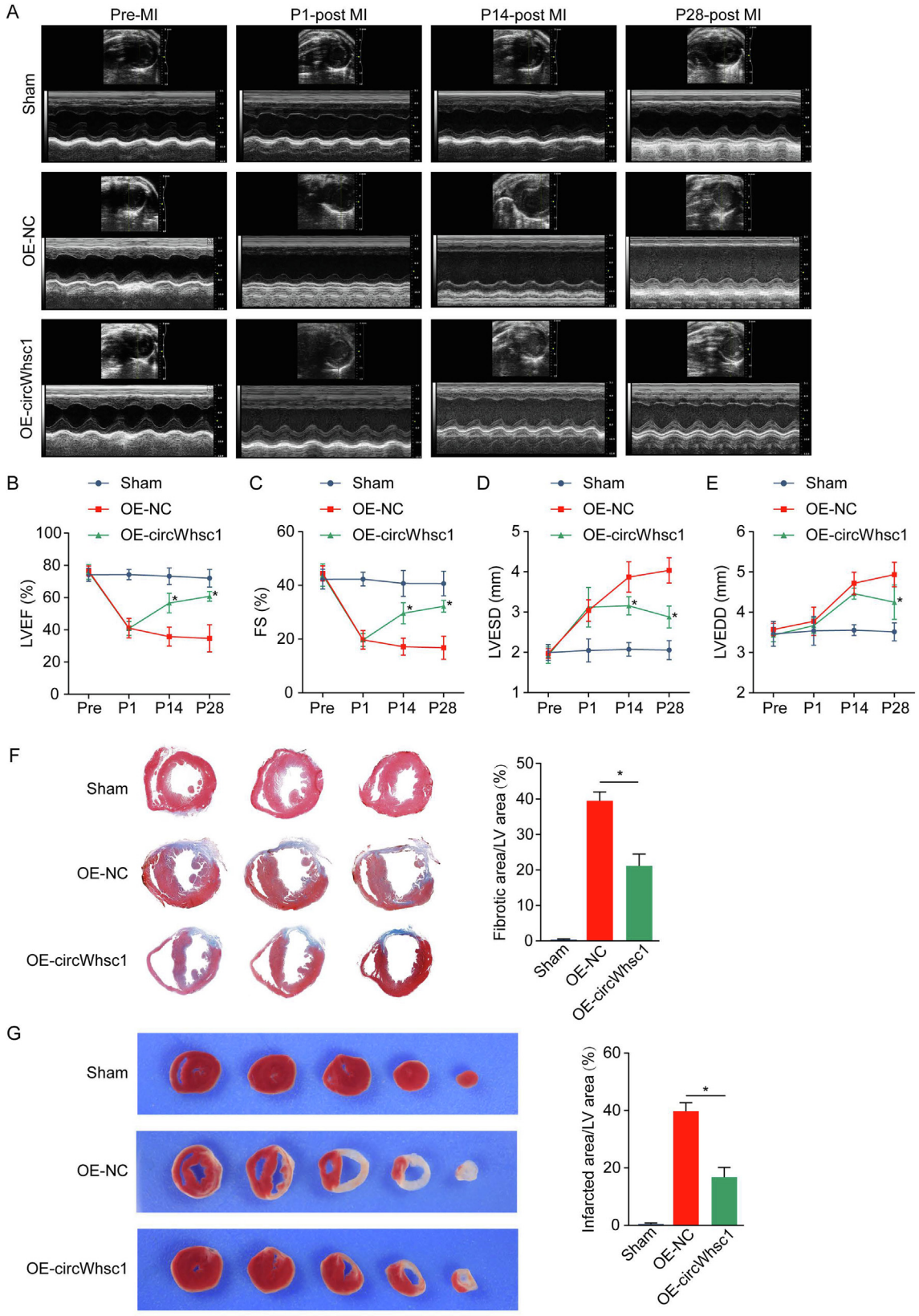

Fig. 4. Cardiac endothelial circWhsc1 overexpression improves cardiac function after MI. (A-E) Cardiac function measured by echocardiography pre-MI and on days 1, 14 and 28 after MI. Representative images (A) and quantitative analysis of left ventricular ejection fraction (LVEF, B), fractional shortening (FS, C), left ventricular end-systolic dimension (LVESD, D) and left ventricular end-diastolic dimension (LVEDD, E) are shown. *P < 0.05 vs the OE-NC group, n = 8. (F) Masson trichrome staining of mouse heart cross sections at 28 days after MI. *P < 0.05, n = 6. (G) Triphenyltetrazolium chloride (TTC) staining of mouse heart cross sections at 28 days after MI. *P < 0.05, n = 6.

tiation 31 (CD31), alpha-smooth muscle actin (α-SMA) and endoglin (CD105) were used to evaluate vascular density, arteriole density and neovascularization, respectively. Immunofluorescence assessment of heart sections 14 days post-MI demonstrated that vascular density and arteriole density in the *peri*-infarcted zone were significantly higher in the AAV2-V_{EC}-circWhsc1 group than in the AAV2-V_{EC}-NC group (Fig. 3E). We also observed greater neovascularization in the border zone in the endothelial-circWhsc1 overexpression group than in the control group (Fig. 3F). Notably, EC circWhsc1 overexpression *in vitro* also benefited angiogenesis, with an increasing ratio of EdU- and pH3-positive ECs observed (Fig. S6A-B). These results suggest that EC-derived circWhsc1 overexpression increases angiogenesis, which might be favorable for cardiac regenerative processes.

As CMs under hypoxia/ischemia conditions have an impact on ECs, it is important to investigate whether CM-EC intercellular communication could stimulate EC to release circWhsc1 under hypoxia/ischemia condition. We performed co-culture of ECs and hypoxia-preconditioned CMs, and then detected circWhsc1 expression in ECs. It was found that circWhsc1 expression was significantly up-regulated in ECs co-cultured with hypoxia-preconditioned CMs, compared to that co-cultured with normoxia-preconditioned CMs (Fig. S6C). Considering the positive correlation between intracellular and EV-RNA content [31], our data indicated that CMs under hypoxia condition might release some kinds of signals that stimulate EC to release CircWhsc1. More detailed studies should be performed to identify these signals.

To determine whether the restoration of cardiac structure was accompanied by improved cardiac function, we performed echocardiographic measurements after MI (Fig. 4A). Echocardiography data of 14 and 28 days after surgery demonstrated significant improvement in left ventricular ejection fraction (LVEF), fractional shortening (FS), left ventricular end-systolic dimension (LVESD) and left ventricular end-diastolic dimension (LVEDD) in mice injected with AAV2-V_{EC}-circWhsc1 compared to those injected with AAV2-V_{EC}-NC (Fig. 4B-E). These beneficial effects were also observed in histological quantification of fibrotic size through Masson trichrome staining (Fig. 4F). Similarly, TTC staining also confirmed that the infarcted area in the endothelial-circWhsc1 overexpression group was significantly smaller than that in the control group (Fig. 4G). Collectively, these results indicate that EC-derived circWhsc1 promotes adult cardiac repair after MI through increased CM proliferation and angiogenesis.

CircWhsc1 deficiency impairs endogenous cardiac regeneration in neonatal rats *in vivo*

To further clarify the proliferative effect of cardiac EC-derived circWhsc1, we utilized an apex resection (AR) model in neonatal rats, which was regarded as a popular animal model for studying heart regeneration [32]. Antisense oligonucleotides (ASOs), a class of synthetic, single-stranded deoxyribonucleotide analogs that are designed to block complementary RNA in a sequence-specific manner, were used in the experiment. ASO-circWhsc1, which was designed to target the back-splicing site of circWhsc1, was synthesized to interfere its expression *in vivo*. *P*1 neonatal rats were subcutaneously injected with ASO-circWhsc1 or scrambled control (ASO-NC). A decreased ratio of Ki67-, pH3-, and Aurora B-positive CMs was observed in the circWhsc1-deficient group compared to the control group (Fig. 5A-C). To investigate the role of circWhsc1 in endogenous cardiac regeneration in neonates, an AR model in *P*1 neonatal rats was utilized. Consistently, we found that injection of ASO-circWhsc1 significantly reduced the ratio of proliferative CM postsurgery compared to ASO-NC (Fig. 5D-F). In addition, immunofluorescence assessment of CD31 and α-SMA demonstrated that vascular density and arteriole density in the *peri*-resected zone were significantly poorer in the ASO-circWhsc1 group than in the control group (Fig. 5G). As evidenced by echocardiography 7 days postsurgery, the LVEF and FS were significantly decreased in the ASO-circWhsc1-treated rats compared to ASO-NC group (Fig. 5H). Moreover, histological analysis of Masson trichrome-stained heart longitudinal sections revealed a remarkably larger fibrotic area in the ASO-circWhsc1 group postsurgery than in the scrambled control group (Fig. 5I). We also performed AR in a *P*1 mouse model, beside a rat model. Consistently, immunofluorescence analysis of Ki67 and pH3 positive CMs in the *peri*-resected zone revealed that proliferative activity was significantly impaired in the ASO-circWhsc1 treated mice postsugery than that in the scrambled control treated mice (Fig. S7A-B). These results highlight that circWhsc1 deficiency postnatally expedites CM cell cycle exit and constrains the postnatal CM proliferative window during the first postnatal week.

CircWhsc1 is packaged into cardiac EC-derived EVs and transported to CMs

Previous studies have demonstrated that EVs play an essential role in mediating cell–cell communications. Thus, we investigated whether EVs mediate the effect of EC-derived circWhsc1 on CM during cardiac regeneration. ECs were transfected with circWhsc1 overexpression adenovirus and then cocultured with CMs. qRT-PCR assays revealed increased expression of circWhsc1 in the lower layer CMs coincubated with circWhsc1-overexpressing ECs compared to the vector group (Fig. 6A). Moreover, immunofluorescence assays revealed a higher rate of proliferative markers in the lower layer CMs coincubated with circWhsc1-overexpressing ECs relative to the vector group (Fig. 6B). However, the proliferative effect of circWhsc1-overexpressing ECs was abolished when ECs were administered GW4869, a small inhibitor of EVs secretion. These results indicate that EVs might act as transport carriers to deliver circWhsc1 from ECs to CMs (Fig. 6A-B).

Next, we collected EVs derived from hypoxia-preconditioned ECs ($EVs^{HP\text{-}EC}$) and normoxia-preconditioned ECs ($EVs^{NP\text{-}EC}$) using the gradient centrifugation method (Fig. S8A). The morphology, size distribution, and marker proteins of EVs were assessed by transmission electron microscopy (TEM), nanoparticle tracking analysis (NTA), and western blot analysis, respectively (Fig. 6C-E). We then used droplet digital PCR (ddPCR) technology to assess circWhsc1 expression in EC derived EVs. We revealed that the expression level of circWhsc1 in $EVs^{HP\text{-}EC}$ was remarkably higher than that in $EVs^{NP\text{-}EC}$ (Fig. 6F). And we also found that circWhsc1 was protected within intact EVs, as evidenced by expression of circWhsc1 not decreasing when EVs were exposed to the RNase A/T1 mix. This protective effect could be eliminated by 1 % Triton X-100, which digests EV membranes (Fig. 6F). Additionally, the circWhsc1 abundance of EVs derived from ECs was notably reduced when they were administered either with siRNA to knockdown circWhsc1 or with GW4869 to inhibit EV secretion. (Fig. 6G-H). We further investigated the effect of ischemic conditions on EC-derived circWhsc1 secretion. CMs were exposed to a combination of serum, glucose, and oxygen deprivation (SGO) to mimic *in vivo* ischemic conditions, as previously described [3,33]. Similarly, we found that EC-derived EV-circWhsc1 expression was significantly upregulated under ischemia condition, compared to the controls (Fig. 6I).

To explore the biological function of circWhsc1 in EC-derived EVs, $EVs^{NP\text{-}EC}$, $EVs^{HP\text{-}EC}$, $EVs^{HP\text{-}EC\text{-}si\text{-}circWhsc1}$ and $EVs^{HP\text{-}EC\text{-}si\text{-}NC}$ were prepared and then coincubated with CMs. The EV uptake experiment of $EVs^{HP\text{-}EC}$ using PKH26, a lipophilic fluorescent dye, showed that EC-derived EVs were taken up by CMs (Fig. 6J). A functional

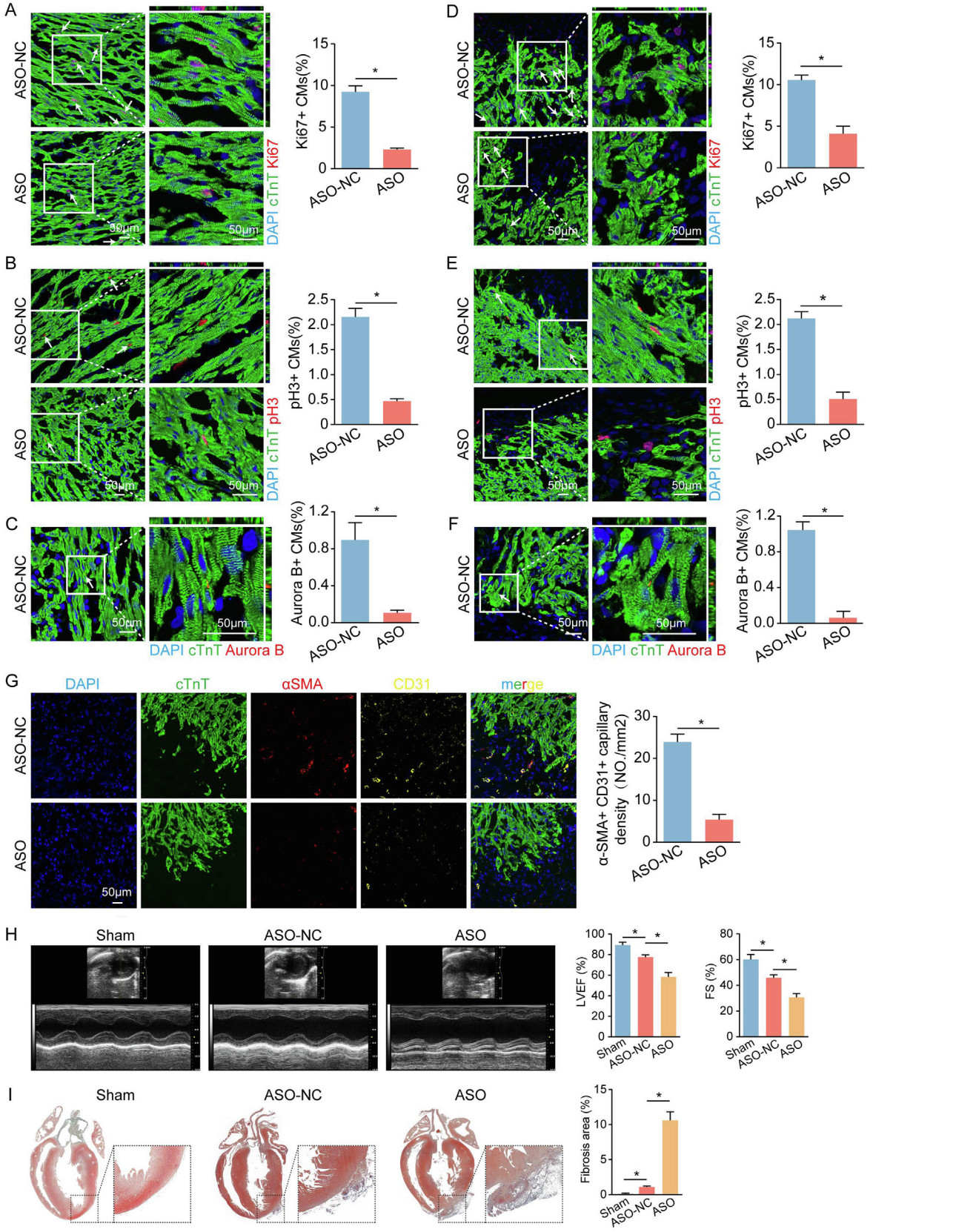

Fig. 5. CircWhsc1 deficiency decreases regenerative repair in neonatal rats *in vivo*. (A-C) Immunofluorescence analysis of Ki67- (A), pH3- (B) and Aurora B- (C) positive CMs in *P*1 neonatal rat heart sections 4 days after ASO-circWhsc1 or ASO-NC administration. CMs are stained with cTnT, nuclei are labeled with DAPI, and proliferating CMs are indicated by arrows, $^{*}P < 0.05$, n = 6. Scale bars, 50 μm. (D-I) *P*1 neonatal rats received an apex resection (AR) model and were administered ASO-circWhsc1 or ASO-NC. Immunofluorescence analysis of Ki67- (D), pH3- (E) and Aurora B- (F) positive CMs in the *peri*-resected zone of heart sections 4 days after ASO-circWhsc1 or ASO-NC administration. Proliferating CMs are indicated by arrows, $^{*}P < 0.05$, n = 6. Scale bars, 50 μm. (G) Immunofluorescence evaluation of CD31 and α-SMA costaining in the *peri*-resected zone of heart sections 4 days after ASO-circWhsc1 or ASO-NC administration. $^{*}P < 0.05$, n = 6. Scale bars, 50 μm. (H) Cardiac function measured by echocardiography 7 days after AR. Quantitative analysis of LVEF and FS. $^{*}P < 0.05$, n = 6. (I) Masson trichrome staining of rat heart sections at 7 days after AR. $^{*}P < 0.05$, n = 6.

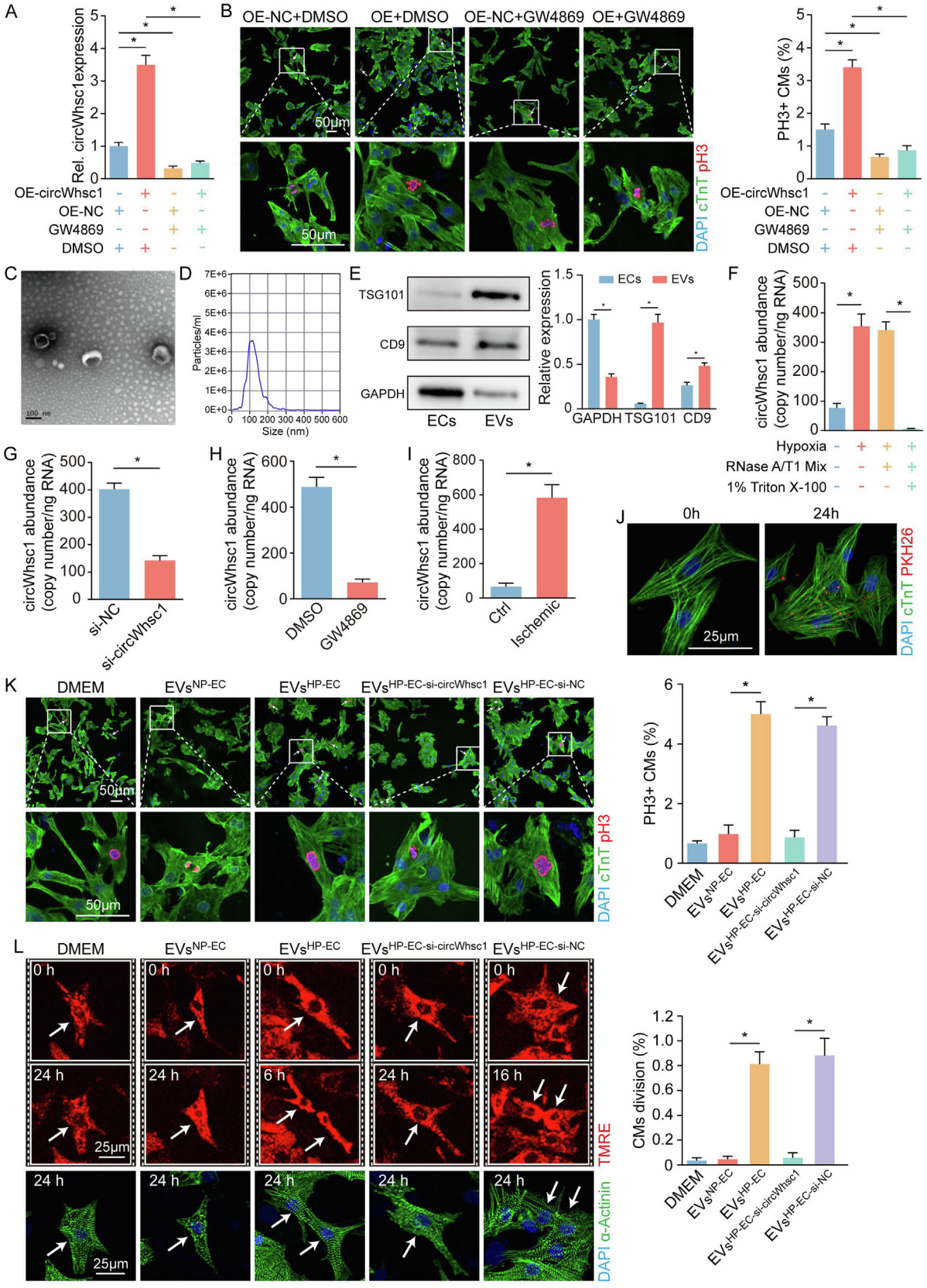
A
Rel. circWhsc1expression
OE-circWhsc1
OE-NC
GW4869
DMSO
B
OE-NC+DMSO
OE+DMSO
OE-NC+GW4869
OE+GW4869
50μm
DAPI cTnT pH3
PH3+ CMs (%)
C
100 nm
D
Particles/ml
Size (nm)
E
TSG101
CD9
GAPDH
ECs
EVs
Relative expression
F
circWhsc1 abundance (copy number/ng RNA)
Hypoxia
RNase A/T1 Mix
1% Triton X-100
G
si-NC
si-circWhsc1
H
DMSO
GW4869
I
Ctrl
Ischemic
J
0h
24h
25μm
DAPI cTnT PKH26
K
DMEM
EVsNP-EC
EVsHP-EC
EVsHP-EC-si-circWhsc1
EVsHP-EC-si-NC
DAPI cTnT pH3
L
0 h
24 h
6 h
16 h
25μm
TMRE
DAPI α-Actinin
CMs division (%)

study showed that EVs^{HP-EC} remarkably promoted cell cycle activity in CM, while silencing circWhsc1 in EVs reduced the above effect on CM cell cycle progression (Fig. 6K, Fig. S8B-C). Moreover, the mitochondrial dye tetramethylrhodamine ethyl ester (TMRE) was utilized to directly obverse dividing CMs. We found that CMs coincubated with EVs^{HP-EC} underwent karyokinesis and cytokinesis. In contrast, almost none of the CMs exhibited cell division activity after coincubation with circWhsc1-deficient EVs (Fig. 6L, Fig. S8D, Supplementary Video S1-5). Moreover, we isolated CMs from adult mouse hearts and investigated whether coculture with EVs^{HP-EC} promotes proliferation in adult mouse CMs. Immunofluorescence assays confirmed that EVs^{HP-EC} coculture also promotes adult CM proliferation with an increased Ki67- and pH3-positive adult CM ratio. Consistently, downregulation of circWhsc1 reversed the effect of EVs^{HP-EC} coculture on adult CM proliferation (Fig. S8E-F). These results indicate that hypoxia-preconditioned EC-derived EV circWhsc1 promotes CM proliferation.

We also investigated whether circWhsc1-coated EVs are sufficient to induce cardiac repair in adult mouse hearts after MI. We overexpressed circWhsc1 in ECs using adenovirus transfection (Fig. S9A). EVs were collected from vector- and circWhsc1- transfected cardiac ECs (EVs^{vector} and EVs^{circWhsc1}), and ddPCR confirmed that circWhsc1 in EVs was up-regulated (Fig. S9B). *In vivo* and *exo vivo* fluorescence of DiR-labeled EVs verified successful delivery of EVs to the heart (Fig. 7A and Fig. S10).

We then intramyocardially injected EVs^{vector} and EVs^{circWhsc1} into *peri*-infarcted area after LAD ligation in 8-week-old mice. Immunofluorescence assays showed that EVs^{circWhsc1} injection significantly increased the ratio of adult CMs expressing proliferative markers, including Ki67 and pH3 (Fig. 7B-C). In addition, immunofluorescence assessment of CD31 and α-SMA demonstrated that vascular density and arteriole density in the *peri*-infarcted zone were significantly enhanced in the EVs^{circWhsc1} group than in the control group (Fig. 7D). Moreover, echocardiographic measurement revealed that cardiac function was significantly improved in EVs^{circWhsc1} group, compared to EVs^{vector} group (Fig. 7E-G). Both Masson trichrome staining and TTC staining confirmed that the infarcted area in EVs^{circWhsc1} group was significantly less than that in EVs^{vector} group (Fig. 7H-I). Altogether, these results indicate that circWhsc1-enriched EVs might be able to promote CM proliferation and cardiac repair in adult mice after MI.

To determine whether the transport of circWhsc1 from ECs to CMs promotes CM proliferation, we directly increased circWhsc1 expression in P7 CMs by transfecting the circWhsc1 overexpression adenovirus. We found that circWhsc1 overexpression increased the ratio of CMs expressing proliferative markers, including EdU, Ki67, pH3 and Aurora B (Fig. S11A-D). Flow cytometry also demonstrated that CMs overexpressing circWhsc1 were more likely to be distributed in the G2/M phases than the control group (Fig. S11E). In addition, qRT-PCR assays revealed that the expression of cell cycle genes was significantly increased in circWhsc1-overexpressing CMs (Fig. S11F).

Previous study has demonstrated that Cx-43 was an important gap function protein acting as the major mediator of intercellular Ca2 + propagation between new CMs and neighboring functioning cardiomyocytes [34]. We performed co-immunostaining of Aurora B and Cx-43 on the circWhsc1-overexpressing CMs and the controls. Accordingly, we found that Cx-43 was also expressed in daughter CMs after circWhsc1 overexpression (Fig. S12). Collectively, these findings suggest that hypoxia induces EC-mediated release of EVs containing circWhsc1 and that EV circWhsc1 is transported from ECs to CMs, which induces CM cell cycle progression.

CircWhsc1 interacts with TRIM59 to activate pTRIM59/pSTAT3/cyclin B signaling in CMs

We next sought to determine the underlying mechanisms by which EV circWhsc1 promotes CM proliferation after transport from ECs. Previous studies have reported that circRNAs often exert their functions often through circRNA-miRNA or circRNA-protein interactions [35]. It was known that the circRNA-miRNA interaction is mediated by the RNA-induced silencing complex (RISC) containing Argonaute2 (Ago2) and many associated proteins. The detection of circRNA from Ago2 RNA RIP-seq assay is believed to examine whether the circRNA candidate could bind to miRNAs [36]. Previous study has performed RIP assays with antibodies against endogenous Ago2 and heat shock protein 90 (Hsp90) as control in CMs [26]. The results showed that circWhsc1 was not enriched in Ago2-rip, compared to Hsp90 (Fig. S13). In contrast, circSlc8a1 and circSnrk, the known miRNA targets in cardiomyocytes, was found to have strong enrichment in the Ago2-RIP but not in the Hsp90-RIP (Fig. S13). These results indicated that circWhsc1 might not function in CMs via sponging miRNA. To screen out proteins that potentially interact with circWhsc1 in CMs, we performed RNA pulldown assays in neonatal mouse CMs using biotinylated probes targeting the circWhsc1 back-splicing sequence. The following mass spectrometry analysis and western blotting assays identified TRIM59, a tripartite motif protein that plays an important role in cell cycle and proliferation, as a protein potentially interacting with circWhsc1(Fig. 8A, Fig. S14A, Supplementary Table S3). Then, the interaction between circWhsc1 and TRIM59 was further validated by RNA immunoprecipitation (RIP)

Fig. 6. Hypoxia-induced ECs promote CM proliferation by delivering EV circWhsc1 to CMs. (A) Relative expression of circWhsc1 in CMs after coculture with ECs. ECs were pretreated with OE-NC + DMSO, OE-circWhsc1 + DMSO, OE-NC + GW4869, and OE-circWhsc1 + GW4869. GW4869 is a small inhibitor of EV secretion. $^*P < 0.05$, n = 4. (B) Representative immunofluorescence images and quantification of pH3-positive CMs after coculture with ECs. ECs were pretreated with OE-NC + DMSO, OE-circWhsc1 + DMSO, OE-NC + GW4869, and OE-circWhsc1 + GW4869. Proliferating CMs are indicated by arrows. $^*P < 0.05$, n = 6. Scale bars, 50 μm. (C) Representative transmission electron microscopy (TEM) images of EVs isolated from the culture medium of HP-ECs. (D) The size distribution of EVs from HP-ECs was analyzed by nanoparticle tracking analysis (NTA). (E) The EV-specific markers TSG101 and CD9 were verified by western blotting analysis. (F) Droplet digital polymerase chain reaction (ddPCR) analysis of circWhsc1 copy numbers in EVs derived from ECs after treatment with RNase A/T1 Mix and 1 % Triton X-100 for 30 min. $^*P < 0.05$, n = 5. (G) DdPCR analysis of circWhsc1 copy numbers in EVs from ECs treated with si-circWhsc1 or si-NC. $P < 0.05$, n = 5. (H) DdPCR analysis of circWhsc1 copy numbers in EVs from ECs treated with GW4869. $^*P < 0.05$, n = 5. (I) DdPCR analysis of circWhsc1 copy numbers in EVs from ECs exposed to ischemic conditions or the controls. $^*P < 0.05$, n = 5. (J) Representative images of the cellular uptake of EVs from HP-ECs after incubation with CMs for 0 hr and 24 hr. Red: EVs dyed with PKH26. Scale bars, 50 μm. (K-L) Neonatal mouse CMs were cultured *in vitro* individually (DMEM) or cocultured with EVs isolated from normoxia-preconditioned ECs (EVs^{NP-EC}), hypoxia-preconditioned ECs (EVs^{HP-EC}), hypoxia-preconditioned ECs treated with si-circWhsc1(EVs$^{HP-EC-si-circWhsc1}$), and hypoxia-preconditioned ECs treated with si-NC (EVs$^{HP-EC-si-NC}$). EVs coculture dosing was quantified by particle number of $1x10^8$. (K) Representative immunofluorescence images and quantification of pH3-positive CMs. $^*P < 0.05$, n = 6. (L) Representative images and quantification and from a 24 hr time-lapse video of P7 CMs cultured individually (DMEM) or incubated with with EVs^{NP-EC}, EVs^{HP-EC}, EVs$^{HP-EC-si-circWhsc1}$ and EVs$^{HP-EC-si-NC}$. The last panel shows immunofluorescence (IF) staining for α-actinin at the 24th hr cells. $^*P < 0.05$, n = 6. Scale bars, 25 μm. (For interpretation of the references to colour in this figure legend, the reader is referred to the web version of this article.)

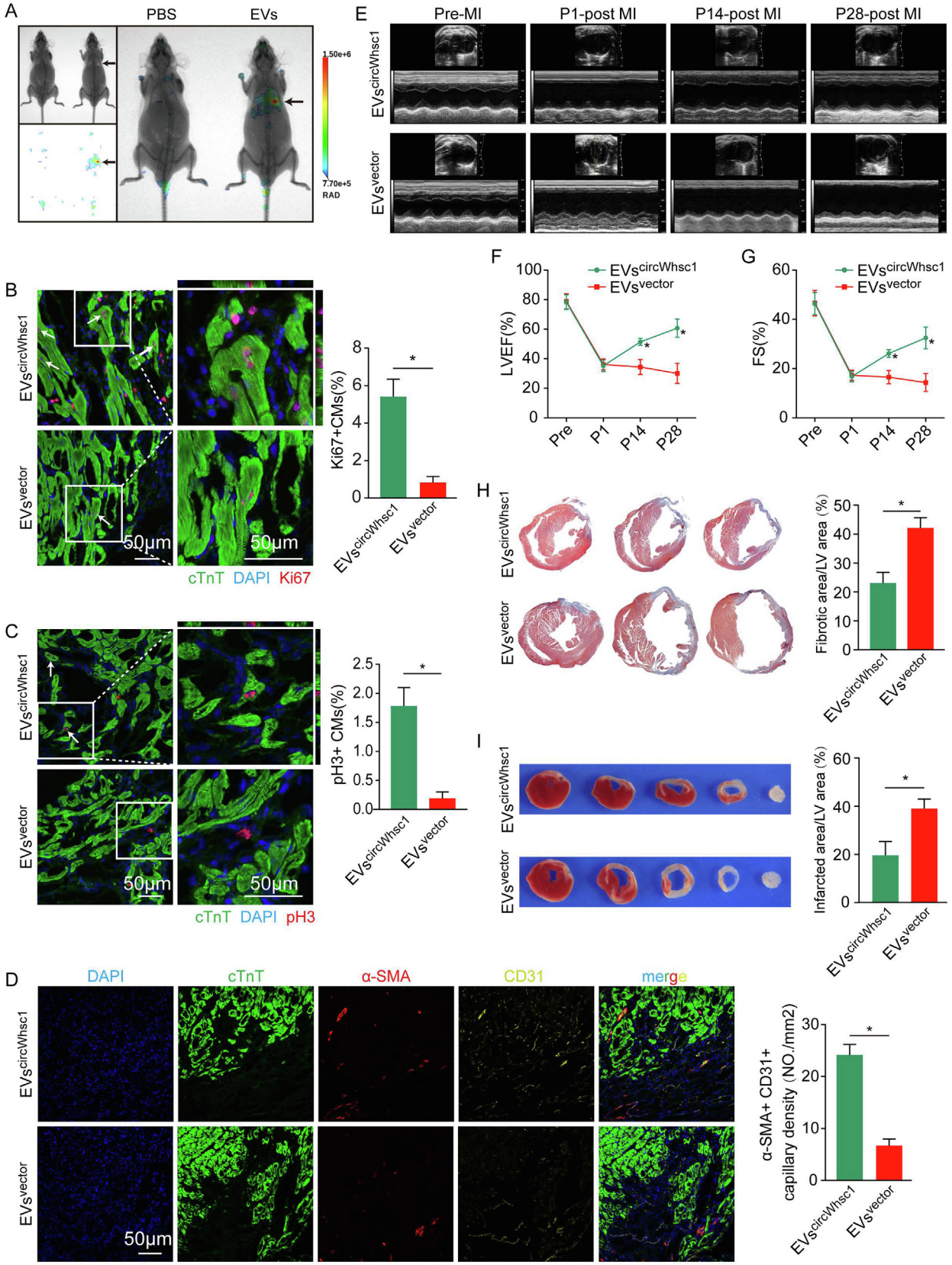

Fig. 7. EV-mediated delivery of circWhsc1 induced CM proliferation and cardiac repair after MI *in vivo*. (A) Representative fluorescence images captured at 2 h after DiR-labeled EVs or PBS intramyocardially injection. EVs delivery dosing was quantified by particle number of $1x10^{10}$. (B-C) Immunofluorescence analysis of Ki67- (B) and pH3- (C) positive adult CMs in the *peri*-infarcted area of heart sections 14 days after $EVs^{circWhsc1}$ or EVs^{vector} administration. CMs are stained with cTnT, nuclei are labeled with DAPI, and proliferating CMs are indicated by arrows, $^*P < 0.05$,n = 6. Scale bars, 50 μm. (D) CD31 and α-SMA costaining in the *peri*-infarcted zone 14 days after $EVs^{circWhsc1}$ or EVs^{vector} injection. $^*P < 0.05$, n = 6. Scale bars, 50 μm. (E-G) Cardiac function measured by echocardiography pre-MI and on days 1, 14 and 28 after MI. Representative images (E) and quantitative analysis of left ventricular ejection fraction (LVEF, F) and fractional shortening (FS, G) are shown. $^*P < 0.05$ vs the EVs^{vector} group, n = 8. (H) Masson trichrome staining of mouse heart cross sections at 28 days after MI. $^*P < 0.05$, n = 6. (I) Triphenyltetrazolium chloride (TTC) staining of mouse heart cross sections at 28 days after MI. $^*P < 0.05$, n = 6.

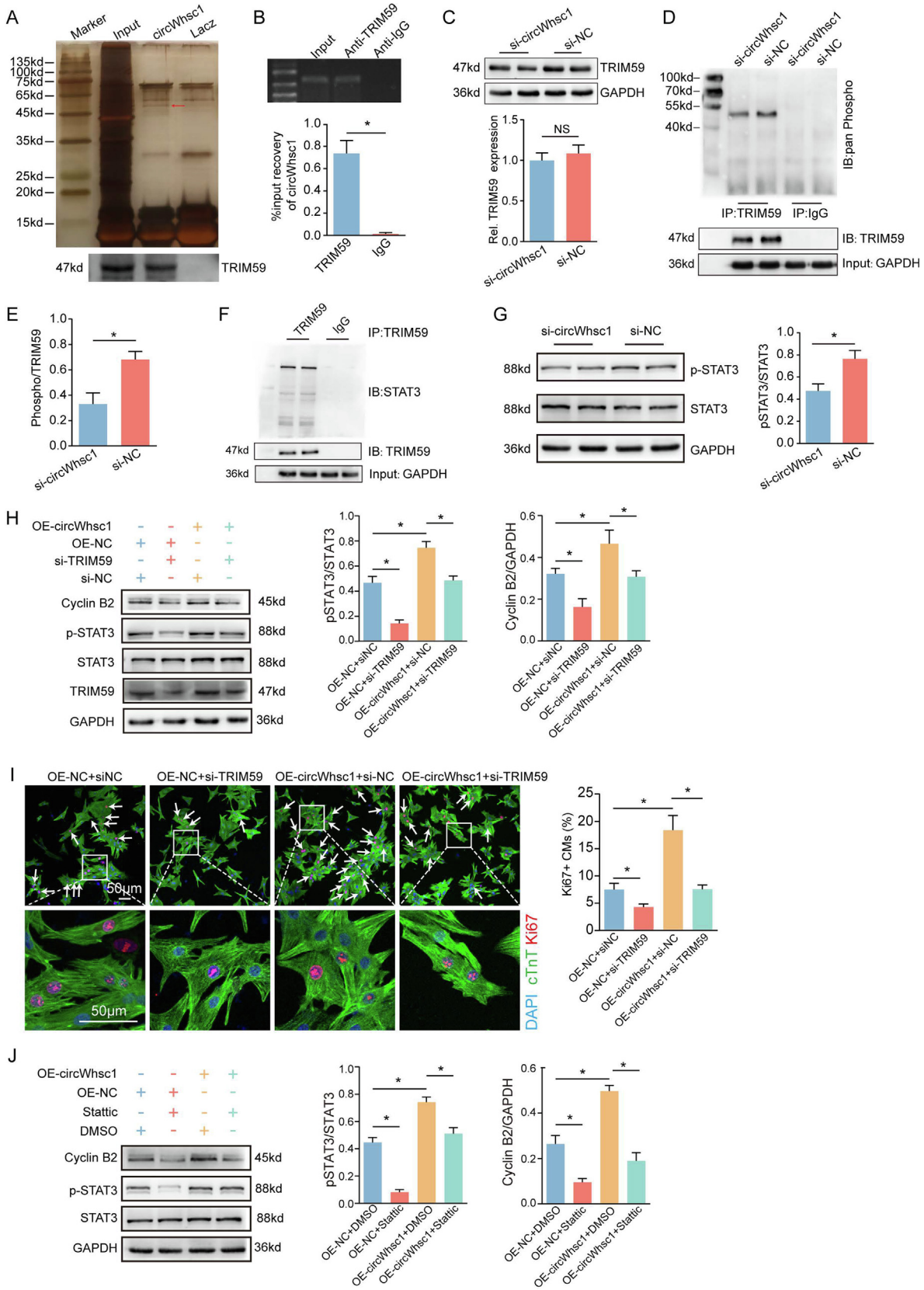
A
Marker
Input
circWhsc1
Lacz
135kd
100kd
75kd
65kd
45kd
35kd
25kd
20kd
15kd
47kd
TRIM59
B
Input
Anti-TRIM59
Anti-IgG
%input recovery of circWhsc1
TRIM59
IgG
C
si-circWhsc1
si-NC
47kd
TRIM59
36kd
GAPDH
Rel. TRIM59 expression
NS
si-circWhsc1
si-NC
D
si-circWhsc1
si-NC
si-circWhsc1
si-NC
100kd
70kd
55kd
40kd
IB:pan Phospho
IP:TRIM59
IP:IgG
47kd
IB: TRIM59
36kd
Input: GAPDH
E
Phospho/TRIM59
si-circWhsc1
si-NC
F
TRIM59
IgG
IP:TRIM59
IB:STAT3
47kd
IB: TRIM59
36kd
Input: GAPDH
G
si-circWhsc1
si-NC
88kd
p-STAT3
88kd
STAT3
36kd
GAPDH
pSTAT3/STAT3
si-circWhsc1
si-NC
H
OE-circWhsc1
OE-NC
si-TRIM59
si-NC
Cyclin B2
45kd
p-STAT3
88kd
STAT3
88kd
TRIM59
47kd
GAPDH
36kd
pSTAT3/STAT3
OE-NC+siNC
OE-NC+si-TRIM59
OE-circWhsc1+si-NC
OE-circWhsc1+si-TRIM59
Cyclin B2/GAPDH
OE-NC+siNC
OE-NC+si-TRIM59
OE-circWhsc1+si-NC
OE-circWhsc1+si-TRIM59
I
OE-NC+siNC
OE-NC+si-TRIM59
OE-circWhsc1+si-NC
OE-circWhsc1+si-TRIM59
50μm
50μm
DAPI cTnT Ki67
Ki67+ CMs (%)
OE-NC+siNC
OE-NC+si-TRIM59
OE-circWhsc1+si-NC
OE-circWhsc1+si-TRIM59
J
OE-circWhsc1
OE-NC
Stattic
DMSO
Cyclin B2
45kd
p-STAT3
88kd
STAT3
88kd
GAPDH
36kd
pSTAT3/STAT3
OE-NC+DMSO
OE-NC+Stattic
OE-circWhsc1+DMSO
OE-circWhsc1+Stattic
Cyclin B2/GAPDH
OE-NC+DMSO
OE-NC+Stattic
OE-circWhsc1+DMSO
OE-circWhsc1+Stattic

assays (Fig. 8B). Bioinformatics analysis also confirmed that circWhsc1 and TRIM59 are likely to interact (Fig. S14B-C).

Subsequently, we assessed the potential effect of the interaction between circWhsc1 and TRIM59 on CM proliferation. The results of western blotting assays showed that circWhsc1 deficiency does not significantly alter TRIM59 protein expression (Fig. 8C). A previous study reported that serine phosphorylation plays an important role in TRIM59 conformational changes and signal transduction [37]. Next, we performed an immunoprecipitation (IP) assay to evaluate whether circWhsc1 affects phosphorylation levels of TRIM59. Our data revealed that circWhsc1 deficiency significantly decreases phosphorylation levels of TRIM59 (Fig. 8D-E), indicating that circWhsc1 might regulate CM proliferation by affecting TRIM59 phosphorylation. Phosphorylated TRIM59 is thought to interact with STAT3 and inhibit dephosphorylation of STAT3 to sustain high levels of p-STAT3, which is closely associated with cell proliferation by regulating cyclin B2. Consistently, we observed the interaction between TRIM59 and STAT3 by co-IP experiments (Fig. 8F). Moreover, we explored whether circWhsc1 affects phosphorylation levels of STAT3 and observed a reduction in p-STAT3 expression in the circWhsc1 downregulation group compared to the control group (Fig. 8G). Next, we performed rescue experiments to confirm the circWhsc1/pTRIM59/pSTAT3 axis. Western blotting results also showed that overexpression of circWhsc1 significantly increases p-STAT3 and cyclin B2 protein levels, which was reversed by inhibiting TRIM59 (Fig. 8H). Moreover, an immunofluorescence assay revealed that upregulation of circWhsc1 increases the ratio of Ki67-positive CMs, which was also blocked by inhibiting TRIM59 (Fig. 8I). Moreover, the increased p-STAT3 and cyclin B2 protein levels and the pH3-positive CM ratio due to circWhsc1 overexpression were also abolished when CMs were treated with stattic, an inhibitor that selectively prevents STAT3 phosphorylation (Fig. 8J, Fig. S15). Collectively, our results indicate that EV circWhsc1 promotes the cell cycle progression of CM by phosphorylating TRIM59, which activates the STAT3 protein and subsequently increases cyclin B2 expression.

Discussion

In this study, we identified hypoxia-induced circRNA-Whsc1 in ECs and demonstrated that it promotes cardiac regeneration and functional recovery post-MI by activating the pTRIM59/pSTAT3/cyclin B2 pathway. Moreover, we revealed that circWhsc1 is secreted by cardiac ECs in an EV-dependent manner to mediate EC-CM interactions during the regenerative process. Our results indicate that EC-derived EV circWhsc1 might be a promising replacement for hypoxia therapy by preserving the hypoxic effect on cardiac regeneration while avoiding general adverse effects.

Our previous studies revealed that circRNA in CMs is involved in endogenous cardiac regeneration [28,38]. The current study demonstrated that EV-derived circRNA functions as a key downstream effector in hypoxia-associated cardiac regeneration, which is meaningful in terms of hypoxia replacement therapy. We found that expression of EC-derived circWhsc1 is closely correlated with environmental hypoxia, similar to its parental gene expression pattern. Functional studies corroborated hypoxia-induced EV circWhsc1 overexpression as an effective and indispensable intercellular proliferative signal for CMs both *in vitro* and *in vivo*. Our results confirmed that EV-derived circWhsc1 plays an important role in regulating CM proliferation, which is partially supported by previous studies that reported the mitogenic role of EV-derived circWhsc1 in other cell types [39–41]. Moreover, hypoxia is a potent modulator of tissue vascularization, which is essential for the survival of both dividing and postmitotic CMs after an infarction insult. Interestingly, we also confirmed that circWhsc1 overexpression promotes EC proliferation and substantially elevates vasculature density in the *peri*-infarct region. The integrative effect of cardiomyogenesis and angiogenesis following circWhsc1 overexpression indicated that it might be a powerful substitute for hypoxia by retaining the hypoxic effect on cardiac repair while avoiding side effects in other tissues. Additionally, our data identified myocardium-specific circWhsc1 expression, which further increased its potential for clinical translation.

Another quite important finding of our study is that EC-derived EVs promote recipient CM proliferation and heart regeneration by mediating EC-CM interactions. Previous studies have reported the important role of endothelial paracrine factors, including Nrg1 and Agrin, in regulating CM functions and homeostasis [30,42,43]. Our study demonstrated that EV-mediated EC-CM interactions exert unique and essential functions in inducing endogenous cardiac regeneration, which has great significance in promoting cardiac repair. First, we found that activation of EV-mediated EC-CM interactions synergistically CM proliferation, as well as angiogenesis, which was regarded as a crucial link to microenvironment remodeling during cardiac regeneration. Our results suggest the potential of EC-derived EVs to adjust the cardiac microenvironment in line with proliferative CMs. Similar to our study, previous research also confirmed that EVs from ECs function in microenvironment establishment during several pathophysiological processes through the coordinated regulation of different cell types [44,45]. Notably, accumulating evidence has shown that directly targeting CM cell cycling, without the support of the cardiac microenvironment, only results in a low regenerative capacity of the myocardium, indicating the indispensable role of the cardiac microenvironment in endogenous cardiac regeneration. EC-derived EVs, a dual functional component controlling CM proliferation and microenvironment remodeling, might effectively facilitate the regenerative capacity of the myocardium. Moreover, EVs have been widely recognized and used as a powerful tool to address the mechanisms underlying disease initiation and progression. Their attractive characteristics, including maximized inherent biological activities from parent cells and good biotolerability, add significant value to the development of regenerative medicine, setting hope for future clinical applications. Taken together, intervening cardiac

Fig. 8. CircWhsc1 regulates CM proliferation by phosphorylating the TRIM59/STAT3/Cyclin B2 pathway. (A) Proteins precipitated by the specific probe targeting the circWhsc1 back-splice site were resolved by SDS-PAGE; lower panel, the TRIM59 protein was detected by western blotting. control probe: lacz. (B) RIP assays revealed that the TRIM59 protein interacts with circWhsc1 in CMs. $^{*}P < 0.05$ vs IgG, n = 4. (C) Western blotting analysis and quantification of TRIM59 protein levels in CMs transfected with si-circWhsc1 or si-NC. GAPDH was used as a loading control. NS, no significance. n = 6. (D-E) Phospho-TRIM59 protein levels in *P*1 CMs transfected with si-circWhsc1 or si-NC assessed by coimmunoprecipitation (co-IP). Protein extract was immunoprecipitated using anti-TRIM59 or control IgG and analyzed by western blotting with anti-phospho antibody. GAPDH was used as a loading control. $^{*}P < 0.05$, n = 6. (F) The interaction between TRIM59 and STAT3 was verified by coimmunoprecipitation (co-IP). Protein extract was immunoprecipitated using anti-TRIM59 or control IgG and was analyzed by western blotting using the anti-Stat3 antibody. GAPDH was used as a loading control. (G) Western blotting analysis and quantification of p-STAT3 protein levels in *P*1 CMs transfected with si-circWhsc1 or si-NC. GAPDH was used as a loading control. $^{*}P < 0.05$, n = 6. (H) Western blotting analysis and quantification of p-STAT3 and cyclin B2 protein levels in *P*1 CMs treated with OE-NC + si-NC, OE-NC + si-TRIM59, OE-circWhsc1 + si-NC or OE-circWhsc1 + si-TRIM59. GAPDH was used as a loading control. $^{*}P < 0.05$, n = 6. (I) Detection of Ki67-positive CMs in *P*1 CMs treated with OE-NC + si-NC, OE-NC + si-TRIM59, OE-circWhsc1 + si-NC or OE-circWhsc1 + si-TRIM59. $^{*}P < 0.05$, n = 6. Scale bars, 50 μm. (J) Western blotting analysis and quantification of cyclin B2 and p-STAT3 protein levels in *P*1 CMs treated with OE-NC + DMSO, OE-NC + Stattic, OE-circWhsc1 + DMSO or OE-circWhsc1 + Stattic. GAPDH was used as a loading control. Stattic, an inhibitor of p-STAT3. $^{*}P < 0.05$, n = 6.

EC-derived EVs might represent a promising strategy for CM proliferation and heart regeneration, and a similar strategy could even be used for the repair process of other tissues.

In current study, we identified the TRIM59/STAT3 signaling pathway as the proliferative effector of EV-derived circWhsc1 in proliferating CMs. The transcription factor STAT3 is the major downstream target of JAK/STAT signaling and is mitogenic in diverse cell types and tissues [46]. When phosphorylated (activated), STAT3 translocates to the nucleus and initiates the transcription of genes involved in cell survival and proliferation [47,48]. Although there is less evidence in CM, it has been reported that early STAT3 activation is indispensable for injury-induced CM proliferation and cardiac regeneration in zebrafish [49]. In addition, the conditioned medium of adipose stromal cells can phosphorylate STAT3 to enhance the proliferation of both NRCMs and adult HL-1 CMs [50]. A recent clinical study also corroborated that STAT3 activation is required to reduce scar size during postconditioning therapy for hypoxic hearts [51]. Recently, two robust studies corroborated TRIM59 as a new mediator of EGFR/STAT3 signaling, wherein TRIM59 directly interacts with STAT3 to prevent the dephosphorylation of STAT3, maintaining STAT3 transcriptional activation to potentiate cell proliferation [37,52]. This evidence lends support to our finding of the mitogenic role of TRIM59/STAT3 in CM proliferation and heart regeneration. Of note, we found that silencing circWhsc1 did not influence expression levels of either TRIM59 or STAT3 but rather improved their phosphorylation flux. Altogether, our study demonstrates that circWhsc1 promotes CM proliferation by activating the mitogenic TRIM59/STAT3 pathway through enhanced phosphorylation flux.

There are several limitations in our study. First, we revealed that environmental hypoxia significantly increased the expression of circWhsc1 in EC-derived EVs. Our findings of enhanced circWhsc1 biogenesis in ECs might explain the change in EV circWhsc1 expression after hypoxia exposure. However, previous studies reported that enrichment of noncoding RNAs in EVs is also associated with the RNA-packaging process. To better understand the link between EV circWhsc1 and hypoxia, whether hypoxia affects the packaging of circWhsc1 into EVs should be explored in the future. Second, this study focused on the association between EC-derived circWhsc1 and CM proliferation. Interestingly, overexpression of EC-derived circWhsc1 promoted angiogenesis in adult mice postinfarction. Considering the indispensable role of angiogenesis in cardiac repair, the mechanism by which circWhsc1 induces angiogenesis should be investigated in the future. Furthermore, we confirmed the transport of EV-derived circWhsc1 from ECs to CMs by detecting circWhsc1 expression in CMs cocultured with EVs from ECs. A luciferase reporter fused with circWhsc1 should be constructed to determine whether circWhsc1 biogenesis process was also affected in CMs in the future.

In conclusion, we demonstrated that EV-mediated transfer of circWhsc1 from hypoxic ECs to CMs induces CM proliferation by activating TRIM59/STAT3 signaling, leading to structural and functional heart recovery in adult mice post-MI. Our findings imply the potential of intercellular circWhsc1 delivery by EVs as a plausible alternative strategy for hypoxia-induced CM supplementation when treating heart diseases with CM loss.

Methods

Model establishment

In this investigation, male C57BL/6J mice that were postnatally aged at 1 day (*P*1), 7 days (P7), and 8 weeks, as well as male Sprague-Dawley (SD) rats at 1 day (*P*1), were employed.

Apical resection (AR) was carried out in *P*1 SD rats and C57 mice as previously mentioned [53]. Briefly, neonatal rats or mice were sedated for several minutes on an ice bed. The heart was then seen after the chest was opened laterally at the fourth intercostal gap. 10 %–15 % of the ventricular apex was removed from the left chamber after the heart had been exteriorized outside the chest. An 8–0 silk suture was used to rapidly close the thoracic wall wounds. The newborn rats or mice were next covered in a warm blanket to rest.

According to earlier studies, MI was carried out on adult mouse hearts [54]. Isoflurane was used to induce and maintain anesthesia in adult mice by inhalation (5 % for induction and 2 % for maintenance). To keep the airway open, the mice were volume-controlled ventilated and endotracheally intubated. The heart was laterally exposed through thoracotomy. An 8–0 silk suture was used to permanently ligate the LAD 2 mm below the left atrium. Mice in the sham group had a similar procedure without having their LADs tied. The chest was shut after that, and the mice were warmed on a blanket until they recovered.

Cell purification and culture

Primary CMs were isolated from *P*1 mice according to an earlier description [55]. Briefly, newly extracted hearts were divided into pieces and digested with 0.25 % trypsin (Gibco, USA) for 12 h at 4 °C. Heart tissue was then further digested for 15 min at 37 °C with 0.1 % type II collagenase (17101–015, Gibco) in 1 % BSA (Sigma, USA). The supernatant was collected and centrifuged, followed by resuspension of the harvested cells in DMEM/F12 medium (Gibco, USA) with 1 % penicillin–streptomycin (P/S) (Gibco, USA) and 10 % FBS. The supernatant was carefully collected and centrifuged once more after two hours of incubation.The cells were then reconstituted in the same medium, seeded onto dishes at the proper density, and incubated at 37 °C in an environment that was humidified and contained 5 % CO_2.

Adult CMs were isolated from 8-week-old mouse hearts as previously described, with a few minor alterations [56]. Briefly, hearts were separated and mounted on a Langendoft device, perfused with calcium-free perfusion buffer for 5 min, and then digested for 10 min with a solution of type II collagenase (15,000 U, Roche) and $CaCl_2$ (50 M). Then, hearts were dissociated gently to separate CMs using a Pasteur pipette. Cells were filtered through a 100 μm strainer and seeded onto culture slides coated with laminin (10 μg/ml, Sigma) in DMEM/F12 medium supplemented with 10 % FBS.

Neonatal or adult cardiac microvascular ECs were isolated as previously described [57,58], with slight alterations. Briefly, shortly after being dissected, mouse hearts were cleaned with sterile PBS, cut into pieces, and digested in 0.25 % trypsin for five minutes at 37 °C. The heart tissue was further digested in 0.1 % type II collagenase at 37 °C after centrifugation. After filtration and centrifugation, the separated cells were washed and resuspended, and then incubated with magnetic beads conjugated with anti-CD31 antibody. Finally, the beads with ECs were washed several times and were ready to use in following applications. Fluorescence with anti-CD31 was used in identification, purity and population of ECs.

Normoxia- or hypoxia- preconditioned ECs were performed by cultured in DMEM/F10 medium (Gibco, USA) with 1 % P/S and 10 % EV-free FBS at 37 °C in a normoxia (with 21 % O_2 and 5 % CO_2) or hypoxic (with 1 % O_2 and 5 % CO_2) environment for 24 hr before coculture or EV isolation. Normoxia- or hypoxia- preconditioned CMs were performed by cultured in DMEM/F10 medium (Gibco, USA) with 1 % P/S at 37 °C in a normoxia (with 21 % O_2 and 5 % CO_2) or hypoxic (with 1 % O_2 and 5 % CO_2) environment for 24 hr before coculture. To mimic ischemic conditions, cultured cells were exposed to hypoxic conditions (O_2: CO_2, 1: 5) and

glucose-free DMEM (Gibco-BRL), without serum supplementary. Medium supplemented with $CoCl_2$ (100 μM, Sigma) was used to mimic a hypoxic environment and was incubated for 24 hr before being cultured in normal EC medium.

Cell and tissue transfection

Small interfering RNA (siRNA) (Ribobio, Guangzhou, China) was utilized to interfere circWhsc1 expression in ECs and CMs, or to interfere TRIM59 expression in CMs. Supplementary Table S2 offers the interference target sequences. A scrambled form was used as the control. Transfections were processed using a Lipofectamine 2000 kit (11668030, Thermo Fisher Scientific) at a final siRNA concentration of 50 nM for 12 h. Further operations were performed 48 hr after transfection.

TIE-driven AAV vectors harboring green fluorescent protein (GFP) for circWhsc1 overexpression in cardiac ECs were obtained from HANBIO (Shanghai, China). Eight-week-old mice were intramyocardially injected at 3–5 sites in the *peri*-infarct zone at a dose of 10^{11} viral genome particles per animal immediately after LAD ligation. Fourteen days post-MI (dpMI), GFP levels in the heart were assessed using immunofluorescence, and circWhsc1 expression levels were detected by RT-qPCR. At 14 and 28 dpMI, cardiac samples were finally collected for detection. In order to achieve circWhsc1 overexpression *in vitro*, CMs and ECs were transduced with Adv-circWhsc1 for 48 h. The multiplicity of infection (MOI) ranged from 10 to 20.

Antisense oligonucleotides (ASOs) specifically targeting circWhsc1 were designed and synthesized by Tsingke Biotechnology Co., ltd. The target sequences are provided in Supplementary Table S2. *P*1 rats were subcutaneously injected with scrambled or circWhsc1 ASO (0.1 μmol/kg) every 2 days after apex resection. Four and seven days after AR, heart tissues were harvested for additional analysis.

Coculture between ECs and CMs

CMs were cultured in the lower chamber of 12- or 24-well plates to a confluency of 80–90 %. ECs were seeded in 0.4 μm pore inserts (Corning), transfected with si-circWhsc1 or si-NC and cultured in normal medium for 24 hr. Then, the inserts were placed above the CMs. Assessments were performed 24 hr after coculture.

EV isolation

EVs from EC-conditioned medium were isolated by ultracentrifugation as previously mentioned [59]. The culture medium was collected for EV isolation after 24 hr of EC culture. The collected supernatant underwent serial centrifugation at 4 °C at 300 × g for 10 min, 2,000 × g for 10 min and 10,000 × g for 30 min and was then filtered through a 0.22 μm filter (Millipore) to eliminate cells and cellular debris. The supernatant was then ultracentrifuged at 110,000 × g for 2 hr at 4 °C (Optima L-80 XP, Beckman Coulter, Brea, CA, USA). After the supernatant was removed as completely as possible, the concentrated final EV pellet was resuspended in PBS and either used immediately or aliquoted and stored at −80 ℃.

EV characterization

EV size distribution and concentration were quantified using NanoSight. EVs were diluted in 0.22 μm filtered sterile PBS (1:100) and injected into the NanoSight instrument. Each individual sample was imaged at least 3 times, recorded for 30 s and analyzed using NTA software (NanoSight, version 3.0).

The morphology of isolated EVs from fresh samples was assessed using transmission electron microscopy (TEM). EVs were fixed in 2 % glutaraldehyde and pipetted onto a formvar/carbon-coated copper grid for 5 min at 25 °C. Then, the grid and sample were dried and contrasted with 2 % uranyl acetate for 1 min at 25 °C. After the grid was washed with PBS and dried off, the images were captured using a Hitachi H7650 transmission electron microscope (Japan).

EC and EV lysates were prepared and analyzed by western blotting (WB). The EV markers TSG101 (AF8259, Beyotime) and CD9 (AF1192, Beyotime) were verified.

EV uptake assay

To assess the uptake of EVs by CMs *in vitro*, EVs from ECs were labeled with the red fluorescent dye PKH26 (MINI26, Sigma) at a final concentration of 8 μM (dye solution), ultracentrifuged twice at 100,000 × g for 70 min, and resuspended in PBS. CMs were seeded into confocal 12-well plates at 1×10^6 cells per well. After culturing for 12 hr, the supernatant medium was replaced with fresh culture medium, and 1×10^8 particles of the PKH26-labeled EVs were added into CMs at 37 °C for 24 hr. The uptake of EVs by CMs was detected using confocal microscopy (Leica).

Coculture of EC-EVs with CMs

CMs were seeded and cultured in 12-well plates at 1×10^6 cells per well. After culturing for 24 hr, the supernatant medium was replaced with fresh culture medium, and 1×10^8 particles of purified EVs from the culture medium of differently treated ECs ($EVs^{NP\text{-}EC}$, $EVs^{HP\text{-}EC}$, $EVs^{HP\text{-}EC\text{-}si\text{-}circWhsc1}$ and $EVs^{HP\text{-}EC\text{-}si\text{-}NC}$) were added to CMs and incubated at 37 °C for 24 hr. Then, CMs were collected for assays.

EV inhibition

EV release was inhibited as previously described [60]. Briefly, ECs were cultured to 80 % confluence in complete DMEM and incubated with 20 μM GW4869 (D1692, Sigma) diluted with 0.05 % DMSO for 24 hr; then, the medium was replaced with EV-free FBS medium containing 20 μM GW4869, and the cells were incubated for another 48 h before the medium was collected for EV isolation or coculture with CMs. Control assessments were performed after treatment with 0.05 % DMSO solution.

EV delivery *in vivo*

To assess EV circWhsc1 delivery to heart *in vivo*, ECs were cultured and transfected with circWhsc1 overexpression adenovirus or vector,then the EVs ($EVs^{circWhsc1}$ and EVs^{vector}) were collected. Eight-week-old mice were intramyocardially injected at 3–5 sites in the *peri*-infarct zone at a dose of $1x10^{10}$ particles EVs per animal immediately after LAD ligation. At 14 and 28 dpMI, heart samples were finally collected for detection.

For EVs fluorescence detection *in vivo*, EVs from ECs were labeled with the red fluorescent dye DiR (D12731, Thermo Scientific), and intramyocardially injected to mouse heart with a dosing of $1x10^{10}$ particles. 2 h after EVs delivery, fluorescence of DiR-labeled EVs were detected using Bruker *In Vivo* FX Pro system (Bruker, MA, U SA).

2,3,5-Triphenyltetrazolium chloride (TTC) staining

TTC assays were carried out in accordance with previously descriptions [28]. Briefly, adult mice were euthanized after

echocardiography detection at 28 dpMI. Mouse hearts were excised and cut into 1.0 mm thick sections using a microtome. The sections were stained with 1 % TTC (T8877, Sigma) at 37 °C for 15 min, fixed in 4 % paraformaldehyde for 10 min and washed with PBS. Slices were scanned, and the infarcted region was evaluated using ImageJ 1.53a (NIH, USA).

Masson trichrome

In adult mice at 28 dpMI or neonatal rats at 7 dpAR, the Masson trichrome staining was used to evaluate the heart fibrotic region. The Masson Trichrome Stain kit (87019, Thermo Scientific) was used to stain sections of a series of levels below the suture (for the AMI group), equivalent levels (for the sham group), or around the apical resection levels (for the AR and sham groups). Using ImageJ software, the amount of collagen deposition (blue) fibrosis was calculated.

Transthoracic echocardiography

Cardiac function was assessed before AMI and at 1, 14, and 28 dpMI in sedated adult mice or assessed at 7 dpAR in neonatal rats (0.4 %-1.5 % isoflurane, RWD) by echocardiography (VisualSonics, Vevo 2100, 30 MHz 550/770 probe). The short axis B-mode was aligned using the mid-papillary muscles, and the heart function was assessed on the M−mode images. The Vevo2100 software was used to process measurements and calculations.

Cell cycle assays

Following the manufacturer's instructions, a cell cycle detection kit was used to evaluate the cell cycle of CMs. Briefly, CMs were isolated and fixed in alcohol at −20 °C for 1 hr. Then, the cells were washed in PBS and treated with RNase A (10 pg) and propidium iodide (5 pg). Cells were examined using flow cytometry (FACScan, BD Biosciences) and were analyzed using FlowJo software.

RNA *in situ* hybridization

After deparaffinization, the slides were incubated in 3 % pepsin diluted in fresh citrate buffer at 37 °C for 30 min and then in prehybridization solution for 2 h at 37 °C, followed by hybridization with DIG-labeled RNA probes (Axl-bio, Guangzhou) at 37 °C overnight. Following a series of SSC buffer washes, Slides were then blocked in 3 % BSA, and incubated in anti–DIG Fab fragments conjugated to alkaline phosphatase for 1 hr at room temperature. Nuclei were counterstained with DAPI solution. The DBM Purple AP substrate (Roche, Basel, Switzerland) was used to detect the hybridized probes.

For fluorescence *in situ* hybridization, a Cy3-labeled specific probe against the circWhsc1 back-splice sequence was designed and synthesized (Axl-bio, Guangzhou). Cells were fixed and permeabilized in 0.5 % Triton X-100. Then, the cells were exposed to hybridization buffer dilute probe for circWhsc1, denatured at 73 °C for 3 min and hybridized overnight at 42 °C in the dark. Nuclei were stained with DAPI solution at room temperature.

Real-time PCR

Total RNA was extracted from cell or tissue lysates using TRIzol (R6830-01E.Z.N. A, OMEGA). Using a nuclear and cytoplasmic RNA purification kit (AM1921, Thermo Scientific), nuclear and cytoplasmic RNA was extracted from cells. PrimeScript RT Master Mix (Takara, Japan) was used with random primers to reverse transcribe RNA into cDNA. RT-PCR for the analysis of gene expression (primer sequences in Supplementary Table S1) was performed using SYBR Green PCR Master Mix (Takara, Japan) in a LightCycler 480 System (Roche, Germany). Expression was normalized to GAPDH or U6 and was evaluated using the 2-ACT method.

Western blotting

Total proteins from cells or tissue lysates were extracted using radioimmunoprecipitation assay (RIPA) lysis buffer containing protease and phosphatase inhibitor. Proteins from each sample were loaded in and separated on 10 % SDS-PAGE gels, followed by transfer onto nitrocellulose membranes. Then, the membranes were blocked in 5 % BSA and incubated with the following primary antibodies overnight at 4 °C: anti-HIF1α (sc-13515, Santa Cruz), anti-TRIM59 (NBP1-59777, Novus Biologicals), anti-STAT3 (sc-8019, Santa Cruz), anti-pSTAT3 (sc-8059, Santa Cruz), anti-Cyclin B2 (AF2509, Beyotime), anti-CD9 (AF1192, Beyotime), anti-Tsg101 (AF8259, Beyotime), and anti-GAPDH (10494–1-AP, Proteintech). The primary antibodies were removed and then washed adequately with TBST buffer. The membranes were incubated with Alexa Fluor 680-conjugated anti-rabbit/mouse immunoglobulin G (IgG; 1:10,000 dilution; Abcam, USA) for 1 h at room temperature. Signals were visualized using Odyssey Software (LI-COR Biosciences, Lincoln, NE, USA). Relative protein expression was calculated using ImageJ analysis software.

Immunoprecipitation (IP) and coimmunoprecipitation (CoIP)

Cell lysates from CMs were diluted in cold lysis buffer containing PMSF and a protease inhibitor cocktail. Protein G-Sepharose beads were added, along with either anti-TRIM59 or IgG, and incubated at 4 °C overnight. After that, lysis buffer was used to thoroughly clean the beads four times. The precipitate was separated using SDS-PAGE and prepared for anti-TRIM59 or anti-IgG antibody WB analysis.

Co-IP assays were carried out using a Co-IP kit (Thermo Scientific Pierce) in accordance with the manufacturer's instructions. Briefly, anti-p-Ser/Phosphoserine (sc-81514, Santa Cruz) or anti-STAT3 (sc-8019, Santa Cruz) was immobilized with resin. Then, lysates were incubated with the antibody-coupled resin at 4 °C for an overnight period. Then, the precipitated complexes were eluted with elution buffer. The eluted proteins were probed by WB analysis using the corresponding antibodies.

Immunofluorescence

Cells or tissue slices were fixed in 4 % paraformaldehyde for half an hour, permeabilized in 0.5 %-1% Triton in PBS for 5–10 min and blocked in 2 % BSA for 1 h at room temperature. The following primary antibodies diluted in 1 % BSA were added to the samples overnight at 4 °C: anti-CD31 (AF3628, R&D Systems), anti-cTnT (ab33589, Abcam), anti-Ki67 (ab15580, Abcam), anti-pH3 (ab170904, Abcam), anti-Aurora B (ab2254, Abcam), anti-Cx-43 (ab11370, Abcam), anti-α-Actinin (ab137346, Abcam), anti-α-SMA (ab5694, Abcam), and anti-CD105 (ab221675, Abcam). The primary antibodies were removed and then washed adequately with PBS. Next, the cells or tissue sections were incubated with fluorescent secondary antibodies for 1 h at room temperature, followed by DAPI staining for 10 min. For EdU staining, a Click-it EdU Imaging Kit (#C10638, Life Technologies) was applied according to the manufacturer's instructions.

Rnase R/actinomycin D

Total RNA (2 μg) extracted from ECs was incubated with 5 U/μg RNase R (R0301, Geneseed) for 20 min at 37 °C, followed by a purification procedure with an RNeasy MinElute Cleanup Kit (Qiagen). ECs were exposed to 2 μg/ml actinomycin D (SBR00013, Sigma) for 0, 8, 16, and 24 hr, at the appointed time the cells were collected, and total RNA was extracted. CircWhsc1 and linear mRNA of Whsc1 expression content was measured by qRT-PCR assays. GAPDH was used as an internal reference.

Time-lapse videos

P7 CMs were isolated and cocultured with EVs in confocal dishes with the aforementioned medium. 24hr after incubation, the cells were stained with the fluorescent mitochondrial-labeling dye tetramethylrhodamine (TMRE, T669, Thermo Fisher Scientific) for 1 hr. Then the CMs were placed in an appropriate environment (21 % O_2, 5 % CO_2, 37℃) and live-cell videos were obtained for continuously 24 hr at an interval of 20 min with a Leica (TCS Sp8) confocal microscope. Immediately after video capture,CMs were fixed with 4 % paraformaldehyde, and followed by immunostaining. anti-α-Actinin (ab137346, Abcam) was used to determine the observed dividing CMs.

RNA pull-down assay

Assays for RNA pull-down were carried out as previously explained [61]. Briefly, cultivated cells were washed in ice-cold PBS, lysed in 0.5 ml buffer, and homogenized. After this, they were incubated at 65 °C for 10 min with biotin-labeled oligonucleotide probes directed against junction sites of circWhsc1. The mixture was next incubated with magnetic beads coated in streptavidin at 4 °C for an overnight period. By including RNase-free BSA and yeast tRNA (Sigma, USA), non-specific RNA–protein interaction was avoided. The RNA-protein bands were washed and eluted from the beads. The retrieved proteins were analyzed by mass spectrometry.

RNA immunoprecipitation (RIP)

RIP was performed as previously described using a Magna RIPTM RNA-binding Protein Immunoprecipitation Kit (Millipore, Stafford, VA) [55]. Magnetic beads coated with TRIM59 antibody (NBP1-59777, Novus Biologicals) and corresponding IgG (A7016, Beyotime) were used to precipitate RNA in CM lysates. qRT-PCR analysis was used to identify the interaction of target RNA.

Droplet digital PCR (ddPCR)

Droplet digital PCR was performed using 10 μL QX200 EvaGreen ddPCR Supermix (#1864033, Bio-Rad), 2 μL cDNA, primer set (final concentration: 100 nM), and ddH_2O, making a 20 μL reaction. The mixture was loaded into a disposable droplet generation cartridge (#1864008, Bio-Rad), and 70 μL droplet generation oil (#1864006, Bio-Rad) was added and placed inside the QX200 droplet generator (#1864002, Bio-Rad). The resulting droplets were transferred to a 96-well plate (#12001925, Bio-Rad), and the plate was heat-sealed with foil followed by PCR. The cycling protocol was as follows: 95 °C for 5 min, then 45 cycles of 95 °C for 30 s, 60 °C for 1 min, 72 °C for 30 s, and final steps at 4 °C for 5 min, 90 °C for 5 min, and final holding at 4 °C. A no-template control (NTC), where cDNA was replaced by nuclease-free water, was included for threshold determination. After PCR, droplets were read in the QX200 Droplet Reader (#1864003, Bio-Rad) and analyzed using Quanta Soft software (#1864011, Bio-Rad).

Statistical analysis

Quantitative data are presented as the mean ± SD. Statistical analysis was performed using SPSS 20.0. software. The Shapiro-Wilk test was used to determine the normality of each dataset. Data that were not normally distributed were subjected to the Mann-Whitney test. Otherwise, statistical analysis between 2 groups was performed using an unpaired Student's *t* test, and differences among multiple groups were assessed using one-way/two-way ANOVA followed by Bonferroni post hoc test. $P < 0.05$ was considered to indicate statistical significance.

Compliance with Ethics requirements

All animal protocols were approved by the animal ethic committee of Nanfang Hospital, Southern Medical University (Approval no. NFYY-2019–0173). All animal experiments were conducted according to the policies instituted by the National Institutes of Health Guide for the Care and Use of Laboratory Animals.

Sources of Funding

This work was supported by the National Natural Science Foundation of China (No. 82070315, No. 82000282, No. 82270509 and No. 82270347); Guangdong Basic and Applied Basic Research Foundation (No. 2019A1515110687 and 2021A1515220026); Guangzhou Basic and Applied Basic Research Fund (No. 202002030198); and Outstanding Youths Development Scheme of Nanfang Hospital, Southern Medical University (No. 2019 J003).

Data availability

CircRNA expression profiles of adult and neonatal rodent hearts were obtained from Werfel et al.'s study (PubMed ID: 27476877). And circRNA expression profiles of EC under hypoxic and normoxic conditions were obtained from Boeckel et al.' study (PubMed ID: 26377962).

Declaration of Competing Interest

The authors declare that they have no known competing financial interests or personal relationships that could have appeared to influence the work reported in this paper.

Appendix A. Supplementary material

Supplementary data to this article can be found online at https://doi.org/10.1016/j.jare.2022.12.014.

References

[1] Karra R, Poss KD. Redirecting cardiac growth mechanisms for therapeutic regeneration. J Clin Invest 2017;127(2):427–36. doi: https://doi.org/10.1172/JCI89786.
[2] Nakada Y, Canseco DC, Thet S, Abdisalaam S, Asaithamby A, Santos CX, et al. Hypoxia induces heart regeneration in adult mice. Nature 2017;541(7636):222–7. doi: https://doi.org/10.1038/nature20173.
[3] Thorp EB. The myocardial unfolded protein response during ischemic cardiovascular disease. Biochem Res Int 2012;2012:. doi: https://doi.org/10.1155/2012/583170583170.
[4] Ye L, Qiu L, Feng B, Jiang C, Huang Y, Zhang H, et al. Role of blood oxygen saturation during post-natal human cardiomyocyte cell cycle activities. Jacc-Basic Transl Sc 2020;5(5):447–60. doi: https://doi.org/10.1016/j.jacbts.2020.02.008.
[5] Dunham-Snary KJ, Wu D, Sykes EA, Thakrar A, Parlow L, Mewburn JD, et al. Hypoxic pulmonary vasoconstriction: from molecular mechanisms to medicine. Chest 2017;151(1):181–92. doi: https://doi.org/10.1016/j.chest.2016.09.001.
[6] Hernandez-Gerez E, Fleming IN. Parson S H A role for spinal cord hypoxia in neurodegeneration. Cell Death Dis 2019;10(11):861. doi: https://doi.org/10.1038/s41419-019-2104-1.

[7] Ischaemic stroke. Nat Rev Dis Primers 2019;5(1):71. doi: https://doi.org/10.1038/s41572-019-0126-8.
[8] Luo Z, Tian M, Yang G, Tan Q, Chen Y, Li G, et al. Hypoxia signaling in human health and diseases: implications and prospects for therapeutics. Signal Transduct Tar 2022;7(1):218. doi: https://doi.org/10.1038/s41392-022-01080-1.
[9] Schönenberger MJ. Kovacs W J Hypoxia signaling pathways: modulators of oxygen-related organelles. Front Cell Dev Biol 2015;3:42. doi: https://doi.org/10.3389/fcell.2015.00042.
[10] Liu Z, Wang Y, Dou C, Xu M, Sun L, Wang L, et al. Hypoxia-induced up-regulation of vasp promotes invasiveness and metastasis of hepatocellular carcinoma. Theranostics 2018;8(17):4649–63. doi: https://doi.org/10.7150/thno.26789.
[11] Fan Q, Mao H, Angelini A, Coarfa C, Robertson MJ, Lagor WR, et al. Depletion of endothelial prolyl hydroxylase domain protein 2 and 3 promotes cardiomyocyte proliferation and prevents ventricular failure induced by myocardial infarction. Circulation 2019;140(5):440–2. doi: https://doi.org/10.1161/CIRCULATIONAHA.118.039276.
[12] Wu B, Zhang Z, Lui W, Chen X, Wang Y, Chamberlain AA, et al. Endocardial cells form the coronary arteries by angiogenesis through myocardial-endocardial vegf signaling. Cell 2012;151(5):1083–96. doi: https://doi.org/10.1016/j.cell.2012.10.023.
[13] Tian Y. Morrisey E E Importance of myocyte-nonmyocyte interactions in cardiac development and disease. Circ Res 2012;110(7):1023–34. doi: https://doi.org/10.1161/CIRCRESAHA.111.243899.
[14] Drawnel FM, Archer CR. Roderick H L The role of the paracrine/autocrine mediator endothelin-1 in regulation of cardiac contractility and growth. Brit J Pharmacol 2013;168(2):296–317. doi: https://doi.org/10.1111/j.1476-5381.2012.02195.x.
[15] Wang W, Mckinnie SM, Patel VB, Haddad G, Wang Z, Zhabyeyev P, et al. Loss of apelin exacerbates myocardial infarction adverse remodeling and ischemia-reperfusion injury: therapeutic potential of synthetic apelin analogues. J Am Heart Assoc 2013;2(4):e249.
[16] Isaac R, Reis F, Ying W. Olefsky J M Exosomes as mediators of intercellular crosstalk in metabolism. Cell Metab 2021;33(9):1744–62. doi: https://doi.org/10.1016/j.cmet.2021.08.006.
[17] Gallet R, Dawkins J, Valle J, Simsolo E, de Couto G, Middleton R, et al. Exosomes secreted by cardiosphere-derived cells reduce scarring, attenuate adverse remodelling, and improve function in acute and chronic porcine myocardial infarction. Eur Heart J 2017;38(3):201–11. doi: https://doi.org/10.1093/eurheartj/ehw240.
[18] Hervera A, De Virgiliis F, Palmisano I, Zhou L, Tantardini E, Kong G, et al. Reactive oxygen species regulate axonal regeneration through the release of exosomal nadph oxidase 2 complexes into injured axons. Nat Cell Biol 2018;20(3):307–19. doi: https://doi.org/10.1038/s41556-018-0039-x.
[19] Bjørge IM, Kim SY, Mano JF, Kalionis B. Chrzanowski W Extracellular vesicles, exosomes and shedding vesicles in regenerative medicine - a new paradigm for tissue repair. Biomater Sci-Uk 2017;6(1):60–78. doi: https://doi.org/10.1039/c7bm00479f.
[20] Wang Y, Liu J, Ma J, Sun T, Zhou Q, Wang W, et al. Exosomal circrnas: biogenesis, effect and application in human diseases. Mol Cancer 2019;18(1):116. doi: https://doi.org/10.1186/s12943-019-1041-z.
[21] Akbar N, Digby JE, Cahill TJ, Tavare AN, Corbin AL, Saluja S, et al. Endothelium-derived extracellular vesicles promote splenic monocyte mobilization in myocardial infarction. JCI. Insight 2017;2(17). doi: https://doi.org/10.1172/jci.insight.93344.
[22] Wu G, Zhou W, Pan X, Sun Z, Sun Y, Xu H, et al. Circular rna profiling reveals exosomal circ_0006156 as a novel biomarker in papillary thyroid cancer. Mol Ther-Nucl Acids 2020;19:1134–44. doi: https://doi.org/10.1016/j.omtn.2019.12.025.
[23] Chen W, Quan Y, Fan S, Wang H, Liang J, Huang L, et al. Exosome-transmitted circular rna hsa_circ_0051443 suppresses hepatocellular carcinoma progression. Cancer Lett 2020;475:119–28. doi: https://doi.org/10.1016/j.canlet.2020.01.022.
[24] Sun J, Li B, Shu C, Ma Q. Wang J Functions and clinical significance of circular rnas in glioma. Mol Cancer 2020;19(1):34. doi: https://doi.org/10.1186/s12943-019-1121-0.
[25] Zhang C, Huo ST, Wu Z, Chen L, Wen C, Chen H, et al. Rapid development of targeting circrnas in cardiovascular diseases. Mol Ther-Nucl Acids 2020;21:568–76. doi: https://doi.org/10.1016/j.omtn.2020.06.022.
[26] Werfel S, Nothjunge S, Schwarzmayr T, Strom T, Meitinger T, Engelhardt S Characterization of circular rnas in human, mouse and rat hearts. J Mol Cell Cardiol 2016;98:103-07. doi: https://doi.org/https://doi.org/10.1016/j.yjmcc.2016.07.007.
[27] Si X, Zheng H, Wei G, Li M, Li W, Wang H, et al. Circrna hipk3 induces cardiac regeneration after myocardial infarction in mice by binding to notch1 and mir-133a. Mol Ther-Nucl Acids 2020;21:636–55. doi: https://doi.org/10.1016/j.omtn.2020.06.024.
[28] Huang S, Li X, Zheng H, Si X, Li B, Wei G, et al. Loss of super-enhancer-regulated circrna nfix induces cardiac regeneration after myocardial infarction in adult mice. Circulation 2019;139(25):2857–76. doi: https://doi.org/10.1161/CIRCULATIONAHA.118.038361.
[29] Boeckel JN, Jaé N, Heumüller AW, Chen W, Boon RA, Stellos K, et al. Identification and characterization of hypoxia-regulated endothelial circular rna. Circ Res 2015;117(10):884–90. doi: https://doi.org/10.1161/CIRCRESAHA.115.306319.
[30] D'Uva G, Aharonov A, Lauriola M, Kain D, Yahalom-Ronen Y, Carvalho S, et al. Erbb2 triggers mammalian heart regeneration by promoting cardiomyocyte dedifferentiation and proliferation. Nat Cell Biol 2015;17(5):627–38. doi: https://doi.org/10.1038/ncb3149.
[31] Tosar JP, Gámbaro F, Sanguinetti J, Bonilla B, Witwer KW. Cayota A Assessment of small rna sorting into different extracellular fractions revealed by high-throughput sequencing of breast cell lines. Nucleic Acids Res 2015;43(11):5601–16. doi: https://doi.org/10.1093/nar/gkv432.
[32] Tao G, Kahr PC, Morikawa Y, Zhang M, Rahmani M, Heallen TR, et al. Pitx2 promotes heart repair by activating the antioxidant response after cardiac injury. Nature 2016;534(7605):119–23. doi: https://doi.org/10.1038/nature17959.
[33] Szegezdi E, Duffy A, O'Mahoney ME, Logue SE, Mylotte LA, O'Brien T, et al. Er stress contributes to ischemia-induced cardiomyocyte apoptosis. Biochem Bioph Res Co 2006;349(4):1406–11. doi: https://doi.org/10.1016/j.bbrc.2006.09.009.
[34] Wang WE, Li L, Xia X, Fu W, Liao Q, Lan C, et al. Dedifferentiation, proliferation, and redifferentiation of adult mammalian cardiomyocytes after ischemic injury. Circulation 2017;136(9):834–48. doi: https://doi.org/10.1161/CIRCULATIONAHA.116.024307.
[35] Liu M, Cao S, Guo Z, Wu Z, Meng J, Wu Y, et al. Roles and mechanisms of circrnas in ovarian cancer. Front Cell Dev Biol 2022;10:1044897. doi: https://doi.org/10.3389/fcell.2022.1044897.
[36] Li Y, Chen B. Huang S Identification of circrnas for mirna targets by argonaute2 rna immunoprecipitation and luciferase screening assays. Methods Mol Biol 2018;1724:209–18. doi: https://doi.org/10.1007/978-1-4939-7562-4_17.
[37] Sang Y, Li Y, Zhang Y, Alvarez AA, Yu B, Zhang W, et al. Cdk5-dependent phosphorylation and nuclear translocation of trim59 promotes macroh2a1 ubiquitination and tumorigenicity. Nat Commun 2019;10(1):4013. doi: https://doi.org/10.1038/s41467-019-12001-2.
[38] Zheng H, Huang S, Wei G, Sun Y, Li C, Si X, et al. Circrna samd4 induces cardiac repair after myocardial infarction by blocking mitochondria-derived ros output. Mol Ther 2022. doi: https://doi.org/10.1016/j.ymthe.2022.06.016.
[39] Liu Y, Chen S, Zong ZH, Guan X. Zhao Y Circrna whsc1 targets the mir-646/npm1 pathway to promote the development of endometrial cancer. J Cell Mol Med 2020;24(12):6898–907. doi: https://doi.org/10.1111/jcmm.15346.
[40] Guan S, Li L, Chen WS, Jiang WY, Ding Y, Zhao LL, et al. Circular rna whsc1 exerts oncogenic properties by regulating mir-7/tab2 in lung cancer. J Cell Mol Med 2021;25(20):9784–95. doi: https://doi.org/10.1111/jcmm.16925.
[41] Zong ZH, Du YP, Guan X, Chen S. Zhao Y Circwhsc1 promotes ovarian cancer progression by regulating muc1 and htert through sponging mir-145 and mir-1182. J Exp Clin Canc Res 2019;38(1):437. doi: https://doi.org/10.1186/s13046-019-1437-z.
[42] Baehr A, Umansky KB, Bassat E, Jurisch V, Klett K, Bozoglu T, et al. Agrin promotes coordinated therapeutic processes leading to improved cardiac repair in pigs. Circulation 2020;142(9):868–81. doi: https://doi.org/10.1161/CIRCULATIONAHA.119.045116.
[43] Bassat E, Mutlak YE, Genzelinakh A, Shadrin IY, Baruch UK, Yifa O, et al. The extracellular matrix protein agrin promotes heart regeneration in mice. Nature 2017;547(7662):179–84. doi: https://doi.org/10.1038/nature22978.
[44] Yue Y, Wang C, Benedict C, Huang G, Truongcao M, Roy R, et al. Interleukin-10 deficiency alters endothelial progenitor cell-derived exosome reparative effect on myocardial repair via integrin-linked kinase enrichment. Circ Res 2020;126(3):315–29. doi: https://doi.org/10.1161/CIRCRESAHA.119.315829.
[45] Song H, Li X, Zhao Z, Qian J, Wang Y, Cui J, et al. Reversal of osteoporotic activity by endothelial cell-secreted bone targeting and biocompatible exosomes. Nano Lett 2019;19(5):3040–308. doi: https://doi.org/10.1021/acs.nanolett.9b00287.
[46] Leibinger M, Zeitler C, Gobrecht P, Andreadaki A, Gisselmann G. Fischer D Transneuronal delivery of hyper-interleukin-6 enables functional recovery after severe spinal cord injury in mice. Nat Commun 2021;12(1):391. doi: https://doi.org/10.1038/s41467-020-20112-4.
[47] Li Z, Song Y, He T, Wen R, Li Y, Chen T, et al. M2 microglial small extracellular vesicles reduce glial scar formation via the mir-124/stat3 pathway after ischemic stroke in mice. Theranostics 2021;11(3):1232–48. doi: https://doi.org/10.7150/thno.48761.
[48] Paris AJ, Hayer KE, Oved JH, Avgousti DC, Toulmin SA, Zepp JA, et al. Stat3-bdnf-trkb signalling promotes alveolar epithelial regeneration after lung injury. Nat Cell Biol 2020;22(10):1197–210. doi: https://doi.org/10.1038/s41556-020-0569-x.
[49] Fang Y, Gupta V, Karra R, Holdway JE, Kikuchi K. Poss K D Translational profiling of cardiomyocytes identifies an early jak1/stat3 injury response required for zebrafish heart regeneration. P Natl Acad Sci Usa 2013;110(33):13416–21. doi: https://doi.org/10.1073/pnas.1309810110.
[50] Przybyt E, Krenning G, Brinker MG. Harmsen M C Adipose stromal cells primed with hypoxia and inflammation enhance cardiomyocyte proliferation rate in vitro through stat3 and erk1/2. J Transl Med 2013;11:39. doi: https://doi.org/10.1186/1479-5876-11-39.
[51] Wu Q, Wang T, Chen S, Zhou Q, Li H, Hu N, et al. Cardiac protective effects of remote ischaemic preconditioning in children undergoing tetralogy of fallot repair surgery: a randomized controlled trial. Eur Heart J 2018;39(12):1028–37. doi: https://doi.org/10.1093/eurheartj/ehx030.
[52] Sang Y, Li Y, Song L, Alvarez AA, Zhang W, Lv D, et al. Trim59 promotes gliomagenesis by inhibiting tc45 dephosphorylation of stat3. Cancer Res 2018;78(7):1792–804. doi: https://doi.org/10.1158/0008-5472.CAN-17-2774.

[53] Mahmoud AI, Porrello ER, Kimura W, Olson EN. Sadek H A Surgical models for cardiac regeneration in neonatal mice. Nat Protoc 2014;9(2):305–11. doi: https://doi.org/10.1038/nprot.2014.021.
[54] Bajpai G, Bredemeyer A, Li W, Zaitsev K, Koenig AL, Lokshina I, et al. Tissue resident ccr2- and ccr2+ cardiac macrophages differentially orchestrate monocyte recruitment and fate specification following myocardial injury. Circ Res 2019;124(2):263–78. doi: https://doi.org/10.1161/CIRCRESAHA.118.314028.
[55] Chen Y, Li X, Li B, Wang H, Li M, Huang S, et al. Long non-coding rna ecrar triggers post-natal myocardial regeneration by activating erk1/2 signaling. Mol Ther 2019;27(1):29–45. doi: https://doi.org/10.1016/j.ymthe.2018.10.021.
[56] Bøtker HE, Hausenloy D, Andreadou I, Antonucci S, Boengler K, Davidson SM, et al. Practical guidelines for rigor and reproducibility in preclinical and clinical studies on cardioprotection. Basic Res Cardiol 2018;113(5):39. doi: https://doi.org/10.1007/s00395-018-0696-8.
[57] Jin Y, Liu Y, Antonyak M. Peng X Isolation and characterization of vascular endothelial cells from murine heart and lung. Methods Mol Biol 2012;843:147–54. doi: https://doi.org/10.1007/978-1-61779-523-7_14.
[58] Luo S, Truong AH. Makino A Isolation of mouse coronary endothelial cells. Jove-J Vis Exp 2016;113. doi: https://doi.org/10.3791/53985.
[59] Jeppesen DK, Fenix AM, Franklin JL, Higginbotham JN, Zhang Q, Zimmerman LJ, et al. Reassessment of exosome composition. Cell 2019;177(2):428–45. doi: https://doi.org/10.1016/j.cell.2019.02.029.
[60] Ibrahim AG, Cheng K. Marbán E Exosomes as critical agents of cardiac regeneration triggered by cell therapy. Stem Cell Rep 2014;2(5):606–19. doi: https://doi.org/10.1016/j.stemcr.2014.04.006.
[61] Song H, Yang Y, Sun Y, Wei G, Zheng H, Chen Y, et al. Circular rna cdyl promotes abdominal aortic aneurysm formation by inducing m1 macrophage polarization and m1-type inflammation. Mol Ther 2022;30(2):915–31. doi: https://doi.org/10.1016/j.ymthe.2021.09.017.